Electronic structure of generic semiconductors: Antifluorite silicide and III-V compounds

D. M. Wood and Alex Zunger
Solar Energy Research Institute, Golden, Colorado 80401
(Received 30 September 1985)

The perturbation potential which transmutes a homopolar column-IV diamondlike semiconductor into either a heteropolar zinc-blende-like III-V or II-VI compound or an antifluorite semiconductor can be thought of as consisting of a sum of two terms: (i) a long-range Coulomb dipole potential $\Delta V_{\rm dip}(\mathbf{r})$ associated with the different valence of the atoms of the compound relative to the atoms in the diamondlike system, and (ii) the remaining, short-range and primarily repulsive core pseudopotential $\Delta V_{\rm CC}(\mathbf{r})$ (a "central-cell" correction). Whereas $\Delta V_{\rm dip}(\mathbf{r})$ is common to all members of a given structural class (e.g., all III-V or all II-VI compounds or all antifluorite silicides), defining thereby generic semiconductors, the central-cell potential $\Delta V_{\rm CC}(\mathbf{r})$ carries the specific signature of each atom, distinguishing therefore members of a given class from each other. Using self-consistent pseudopotential band theory within the local-density formalism, we calculate the band structures, equilibrium lattice constants, and electronic charge densities of a generic III-V compound and an antifluorite silicide, distinguishing those aspects of the electronic structure which are generic to a given class from those which are a consequence of the central-cell effects associated with given atoms. The antifluorite materials $Mg_2X^{\rm IV}$ with X^{IV}=Si,Ge,Sn,Pb and Be_2C may be usefully regarded as "filled tetrahedral structures" (FTS's), i.e., consisting of a zinc-blende $M^{\rm II}X^{\rm IV}$ substructure (for $M^{\rm II}$=Be,Mg) one of whose two inequivalent classes of tetrahedral interstitial sites is occupied by an additional $M^{\rm II}$ atom. Pursuing this FTS interpretation, we follow the continuous evolution of the electronic structure and total energy of Si into those of Mg_2Si in terms of $\Delta V_{\rm dip}(\mathbf{r})$ and $\Delta V_{\rm CC}(\mathbf{r})$. Retention of $\Delta V_{\rm dip}(\mathbf{r})$ alone causes the resulting material to be metallic (hence, generic Si antifluorite compounds are metals), whereas the effects of the central-cell perturbation for Mg_2Si largely compensate those of the dipole potential as far as the band structure is concerned, rendering Mg_2Si a semiconductor. Results for our decomposition of antifluorite compounds into $\Delta V_{\rm dip}(\mathbf{r})+\Delta V_{\rm CC}(\mathbf{r})$ are compared with the more familiar transmutation of Si into a generic III-V or II-VI compound, where central-cell effects are found to be responsible for small variations in the lattice parameters within the III-V series.

I. INTRODUCTION

Many of the covalently bonded cubic octet tetrahedral semiconductors can be described as a face-centered-cubic (fcc) Bravais lattice with primitive translation vectors $\mathbf{a}_1=a(0,\frac{1}{2},\frac{1}{2})$, $\mathbf{a}_2=a(\frac{1}{2},0,\frac{1}{2})$, and $\mathbf{a}_3=a(\frac{1}{2},\frac{1}{2},0)$ (where a is the cubic lattice constant) and the specification of the occupation of four inequivalent basis sites within the primitive cell, denoted[1]

$$\begin{aligned}
&\tau_1=a(0,0,0);\ \text{site } S1\\
&\tau_2=a(\tfrac{1}{4},\tfrac{1}{4},\tfrac{1}{4});\ \text{site } S2\\
&\tau_3=a(\tfrac{1}{2},\tfrac{1}{2},\tfrac{1}{2});\ \text{site } I3\\
&\tau_4=a(\tfrac{3}{4},\tfrac{3}{4},\tfrac{3}{4});\ \text{site } I4\ .
\end{aligned}\qquad (1)$$

Each site $i=1,2,3,4$ is coordinated by eight neighboring sites with a nearest-neighbor bond length $a\sqrt{3}/4$ (Fig. 1). In the diamond lattice both substitutional (S) sites $S1$ at τ_1 and $S2$ at τ_2 are occupied by identical atoms, whereas the two interstitial (I) sites $I3$ at τ_3 and $I4$ at τ_4 are vacant. The space group is then O_h^7 ($Fd3m$), having inversion symmetry about $(\tau_1+\tau_2)/2$. In the zinc-blende structure of III-V and II-VI compounds, the cation C occurs at τ_1, the anion A at τ_2, and both the interstitial

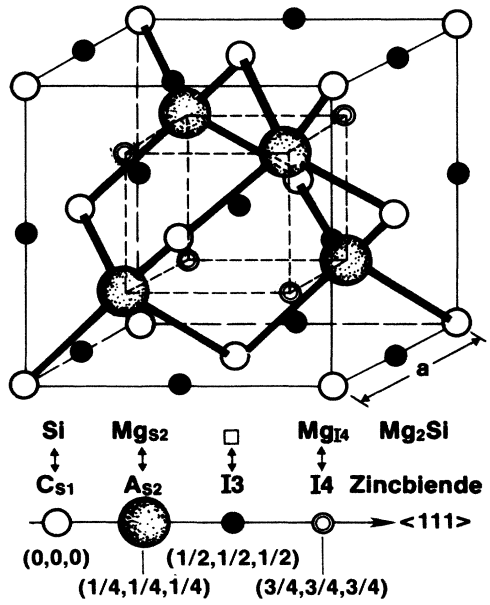

FIG. 1. Crystal structure of zinc-blende and antifluorite compounds depicting substitutional and interstitial sites; Mg sublattice indicated via dashed lines.

sites—τ_3 nearest the anion and τ_4 nearest the cation—are vacant (Fig. 1). The space-group symmetry is then reduced to T_d^2 ($F\bar{4}3m$).

There exists a large and interesting class of materials characterized as filled tetrahedral structures[1] (FTS's) in which, in addition to the occupation of the *substitutional* sites τ_1 and τ_2, one or both of the two *interstitial* sites τ_3 and τ_4 are occupied by "stuffing atoms". The Nowotny-Juza compounds[2] $A^{\rm I}B^{\rm II}C^{\rm V}$, where $B^{\rm II}$=Be,Mg,Zn,Cd occupies the τ_1 site, $C^{\rm V}$=N,P,As,Sb,Bi occupies τ_2, and $A^{\rm I}$=Li,Cu,Ag occupies the interstitial site τ_3 (or is statistically distributed between τ_3 and τ_4), constitute a subclass of the FTS which we have recently discussed.[3,4] The $L2_1$ Heusler alloys[5] $A_2{\rm Mn}B$ (where A=Co,Ni,Cu,Pd and B=Al,In,Sb,Sn) and the $B32$ Zintl compounds of the LiAl (Ref. 6) type (with Li on the sites τ_1 and τ_3, and Al on τ_2 and τ_4) can, similarly, be regarded as FTS. Another group of materials belonging to the FTS class are the antifluorite compounds[7] (denoted generally as $M_2^{\rm II}X^{\rm IV}$) Be_2C and $Mg_2X^{\rm IV}$ [space group $Fm3m$ (O_h^5)], where $X^{\rm IV}$=Si,Ge,Sn,Pb. This structure has an $X^{\rm IV}$ atom at τ_1, an $M^{\rm II}$ atom at τ_2 (denoted, for example, as Mg_{S2}) and a second $M^{\rm II}$ atom at τ_4 (denoted, for example, by Mg_{I4}); the $M^{\rm II}$ atoms therefore comprise an interpenetrating simple cubic lattice of lattice constant $a/2$; see Fig. 1. Whereas $X^{\rm IV}$ is fourfold coordinated in the $X^{\rm IV}X^{\rm IV}$ diamond structure, it is eightfold coordinated in $M_2^{\rm II}X^{\rm IV}$. These antifluorite compounds have much in common with the more familiar group-IV diamond (two divalent $M^{\rm II}$ metallic atoms replacing a single tetravalent $X^{\rm IV}$ atom) and the III-V and II-VI zinc-blende semiconductors, including eight valence electrons per molecule (and hence four valence bands) and an overall similarity of the electronic structure since the Bravais lattices and hence Brillouin zones are identical for these classes. Among the antifluorite compounds only Mg_2Pb is found experimentally[8] to be metallic, the rest being indirect gap semiconductors,[7] with indirect ($\Gamma_{15v}\rightarrow X_{1c}$ or $\Gamma_{15v}\rightarrow X_{3c}$) and direct ($\Gamma_{15v}\rightarrow\Gamma_{1c}$) band gaps, respectively, of $\sim$0.6 and 2.17 eV for Mg_2Si, 0.74 and 1.64 eV for Mg_2Ge, 0.36 and $\sim$1.2 eV for Mg_2Sn, and ~-0.15 eV for the indirect (negative) band gap of Mg_2Pb. They have been studied experimentally[7] via x-ray diffraction,[9] photoemission spectroscopy,[10] electroreflectance[11] and reflectivity,[12] and theoretically using Hartree-Fock[13] and empirical pseudopotential techniques.[14–16] Be_2C has recently been examined theoretically.[17]

In earlier papers[3,4] we have discussed the range of properties observed for the large and interesting class of filled tetrahedral structures and provided a rule for understanding the distortions induced in the electronic structure of the underlying zinc-blende parent by certain types of stuffing atom. Our purpose in this paper will be threefold: (1) to present the first nonempirical total-energy and band-structure calculation for Mg_2Si; (2) to understand the features of the electronic structure of Mg_2Si in the light of the behavior of other FTS, having indicated above the mapping of the Mg_2X antifluorite materials onto the FTS, and (3) to illustrate the results of an interesting decomposition of general applicability (motivated by this mapping) of the "transmutation potential" which converts in a continuous fashion a diamondlike structure into either its antifluorite analog $M_2^{\rm II}X^{\rm IV}$, or into a zinc-blende-type binary compound.

II. CONCEPTUAL FRAMEWORK OF CALCULATION

A. General formalism

Given the similarity between the electronic structures of the antifluorite silicides and the diamondlike or zinc-blende semiconductors, it is natural to seek an understanding of such differences as exist in terms of the differences in the external one-body potentials in which the valence electrons move. Within the density functional framework, the total crystal potential $V_{\rm cry}(\mathbf{r})$ in which electrons move consists of the bare external potential $V_{\rm ext}(\mathbf{r})$ and the screening potential $V_{\rm scr}[\rho(\mathbf{r})]$ induced in the system with electronic charge density $\rho(\mathbf{r})$ by this bare potential,

$$V_{\rm cry}(\mathbf{r})=V_{\rm ext}(\mathbf{r})+V_{\rm scr}[\rho(\mathbf{r})]\ . \tag{2a}$$

For this potential one-electron eigenstates $\psi_{n\mathbf{k}}(\mathbf{r})$ of Bloch form with eigenvalues $\varepsilon_{n\mathbf{k}}$ are defined by the single-particle Schrödinger equation

$$[-\tfrac{1}{2}\nabla^2+V_{\rm cry}(\mathbf{r})]\psi_{n\mathbf{k}}(\mathbf{r})=\varepsilon_{n\mathbf{k}}\psi_{n\mathbf{k}}(\mathbf{r}) \tag{2b}$$

and from which the density $\rho(\mathbf{r})$ is defined via

$$\rho(\mathbf{r})=\sum_{n}^{\rm occ}\sum_{\mathbf{k}}N_{n\mathbf{k}}\,|\,\psi_{n\mathbf{k}}(\mathbf{r})\,|^2\ , \tag{2c}$$

where "occ" indicates occupied states of wave vector $\mathbf{k}$ and band index n within the Brillouin zone, and $N_{n\mathbf{k}}$ is the corresponding occupation number. For a given external potential $V_{\rm ext}(\mathbf{r})$ (which also specifies the structure and its parameters) self-consistent solutions for the screening $V_{\rm scr}[\rho(\mathbf{r})]$, the ground-state density $\rho(\mathbf{r})$, and the total energy $E_{\rm tot}$ can be sought.

The external potential $V_{\rm ext}(\mathbf{r})$ can be formulated either within an all-electron (ae) or within a pseudopotential (ps) framework. In the absence of imposed external fields the all-electron external potential, set up by the nuclear charges Z_α, is given by

$$V_{\rm ext}^{\rm ae}(\mathbf{r})=\sum_{\tau_\alpha}\sum_{\mathbf{R}}-Z_\alpha/\,|\,\mathbf{r}-\mathbf{R}-\tau_\alpha\,|\ , \tag{3}$$

where the $\mathbf{R}$ span the Bravais lattice and the site vectors $\{\tau_\alpha\}$ are the positions of the inequivalent sites α of atomic number Z_α within the primitive cell [Eq. (1)]. In a first-principles pseudopotential formalism (e.g., Refs. 18 and 19), the external crystal potential $V_{\rm ext}^{\rm ps}(\mathbf{r})$ in which the valence electrons move can be expressed as a superposition of angular-momentum l-dependent (i.e., nonlocal) atomic pseudopotentials $w_{\alpha,l}(r)$,

$$V_{\rm ext}^{\rm ps}(\mathbf{r})=\sum_{\tau_\alpha}\sum_{\mathbf{R}}\sum_{l}w_{\alpha,l}(\mathbf{r}-\mathbf{R}-\tau_\alpha)\hat{P}_{l,\alpha}\ , \tag{4}$$

where $\hat{P}_{l,\alpha}$ is a projection operator for angular momentum l about the basis site τ_α. One may in general decompose the pseudopotential into an attractive l-independent long-range Coulomb contribution and the remaining nonlocal,

necessarily short-range and generally repulsive (R) contribution,[18]

$$w_{\alpha,l}(r) \equiv -Z_\alpha^v/r + v_{\alpha,l}^R(r) \ . \tag{5}$$

Here Z_α^v is the nominal valence (v) charge of the atom (e.g., $Z_{\rm IV}^v=4$, $Z_{\rm II}^v=2$) and is hence common to all elements belonging to the same column of the periodic table. The properties peculiar to *different* atoms belonging to the same column in the periodic table are carried by the "repulsive" core potential $v_{\alpha,l}^R(r)$, which depends on angular momentum l, reflecting the different scattering power of a given atomic core for valence electrons of different angular momentum l.[18,19] The characteristic scale over which it is appreciable is a "core radius" (typically smaller than the covalent atomic radius) whose size is dictated by the requirements of orthogonality of a valence electron state of angular momentum l to core states of the same l. Characteristically, states l with no counterparts of the same l in the core (e.g., $l=1$ in first row atoms, $l=2$ in the $3d$ series) have a very weak (or vanishing) $v_{\alpha,l}^R(r)$ [hence , a strong, nearly Coulombic $w_{\alpha,l}(r)$], and those with core states of the same l have $v_{\alpha,l}^R(r)>0$ [hence, a weak overall potential $w_{\alpha,l}(r)$, as is the case for K,Rb,Cs]. Furthermore, the $v_{\alpha,l}^R(r)$ for atoms having the same core configuration (i.e., isocoric atoms such as Mg and Si) vary smoothly across a row of the periodic table.[18] This decomposition, within the pseudopotential formalism, is of general validity; the behavior for small r of $w_{\alpha,l}(r)$ divides pseudopotentials into the so-called "hard-core" [$w_{\alpha,l}(r)\to\infty$ as $r\to 0$] and "soft-core" [$w_{\alpha,l}(r)\to$const as $r\to 0$] varieties. With the decomposition Eq. (5) we may write Eq. (4) analogously as

$$V_{\rm ext}^{\rm ps}(\mathbf{r}) = \sum_{\mathbf{R}}\sum_{\tau_\alpha} -Z_\alpha^v/|\mathbf{r}-\mathbf{R}-\tau_\alpha| + \sum_{\mathbf{R}}\sum_{\tau_\alpha}\sum_l v_{\alpha,l}^R(\mathbf{r}-\mathbf{R}-\tau_\alpha)\hat{P}_{l,\alpha} \ . \tag{6}$$

Note that while the bare *atomic* pseudopotential Eq. (5) is *fixed* for a given atom, the crystal pseudopotential [Eqs. (4) and (6)] depends on the lattice constant and the crystal structure though $\mathbf{R}$ and τ_α.

B. Decomposition of the external crystal potential for antifluorite silicides

Using the description of $V_{\rm ext}^{\rm ps}(\mathbf{r})$ of Eq. (6) it is now possible to relate the external potential for a compound (e.g., $M_2^{\rm II}X^{\rm IV}$) to that of its homopolar analog (e.g., $X^{\rm IV}X^{\rm IV}$), defining thereby the components of the perturbation transforming one into the other. Recalling (see Fig. 1) that in both the diamond structure $X^{\rm IV}X^{\rm IV}$ and antifluorite structure $M_2^{\rm II}X^{IV}$ the substitutional site τ_1 [Eq. (1)] is occupied by the same atom $X^{\rm IV}$, we may write

$$V_{\rm ext}^{\rm ps}(M_2^{\rm II}X^{\rm IV}) \equiv V_{\rm ext}^{\rm ps}(X^{\rm IV}X^{\rm IV}) + \Delta V_{\rm dip}(\mathbf{r}) + \Delta V_{\rm CC}(\mathbf{r}) \ . \tag{7}$$

Here the dipole perturbation $\Delta V_{\rm dip}(\mathbf{r})$ results from the mismatch in atomic valence charge on sites τ_2 and τ_4 [first term of Eq. (6)], i.e.,

$$\Delta V_{\rm dip}(\mathbf{r}) = \sum_{\mathbf{R}} (\Delta Z_{S2}^v/|\mathbf{r}-\mathbf{R}-\tau_2| + \Delta Z_{I4}^v/|\mathbf{r}-\mathbf{R}-\tau_4|) \equiv \Delta V_{\rm dip}^{S2}(\mathbf{r}) + \Delta V_{\rm dip}^{I4}(\mathbf{r}) \ , \tag{8}$$

where $\Delta Z_{S2}^v = Z_{\rm II}^v - Z_{\rm IV}^v = -2$ and $\Delta Z_{I4}^v = Z_{\rm II}^v = +2$. The negative end of the dipole sets up a perturbation $\Delta V_{\rm dip}^{S2}(\mathbf{r})$ and resides at $S2$ while the positive end sets up the perturbation $\Delta V_{\rm dip}^{I4}(\mathbf{r})$ and resides at $I4$ [cf. Eq. (1)]. $\Delta V_{\rm dip}(\mathbf{r})$ is common to all $M_2^{\rm II}X^{\rm IV}$ antifluorite compounds and reduces the space-group symmetry from O_h^7 to T_d^2. We therefore refer to the fictitious compound characterized by the external potential $V_{\rm ext}^{\rm ps}(X^{\rm IV}X^{\rm IV})+\Delta V_{\rm dip}(\mathbf{r})$ as the "generic antifluorite" corresponding to the parent $X^{\rm IV}X^{\rm IV}$ homopolar analog. The third term of the right-hand side of Eq. (7) represents the differences in repulsive core potentials for $M^{\rm II}$ and $X^{\rm IV}$ atoms as well as for an $M^{\rm II}$ atom and vacuum. It is given by the "central-cell" (CC) perturbation potential [second term of Eq. (6)]

$$\Delta V_{\rm CC}(\mathbf{r}) = \sum_{\mathbf{R}}\sum_l [v_{{\rm II},l}^R(\mathbf{r}-\mathbf{R}-\tau_2) - v_{{\rm IV},l}^R(\mathbf{r}-\mathbf{R}-\tau_2)] + \sum_{\mathbf{R}}\sum_l v_{{\rm II},l}^R(\mathbf{r}-\mathbf{R}-\tau_4) \equiv \Delta V_{\rm CC}^{S2}(\mathbf{r}) + \Delta V_{\rm CC}^{I4}(\mathbf{r}) \ . \tag{9}$$

This term distinguishes different $M_2^{\rm II}X^{\rm IV}$ antifluorite compounds belonging to the same generic group. For later reference we have broken $\Delta V_{\rm CC}$ into components labeled $S2$ on the substitutional τ_2 site and $I4$ on the interstitial τ_4 site. Notice that $\Delta V_{\rm dip}(\mathbf{r})$ of Eq. (8) is analogous to the long-range Coulomb potential set up by a nonisovalent impurity in a crystal and that $\Delta V_{\rm CC}(\mathbf{r})$ of Eq. (9) is analogous to the central-cell corrections for such an impurity.[20] In point-ion effective-mass theory,[20] the first term is common to all impurities belonging to the same column whereas the second term is responsible for the variations in their chemical trends. In contrast to impurity theory, $\Delta V_{\rm dip}(\mathbf{r})$ and $\Delta V_{\rm CC}(\mathbf{r})$ are periodic functions. Figures 2(a)–2(d) depict, in the (110) plane of the fcc Bravais lattice, the four potential terms appearing in Eq. (7) (calculated in a manner to be described below), evaluated at the common lattice constant $a=6.338$ Å, the experimentally observed[7] lattice constant of Mg_2Si; in this and later figures, negative function values are indicated as dashed contours. The detailed interpretation of this figure will be deferred to Sec. IV.

With the notation established above we are in a position to ask how the electronic structure of $M_2^{\rm II}X^{\rm IV}$ (e.g., Mg_2Si) evolves from that of $X^{\rm IV}X^{\rm IV}$ (e.g., Si) as the dipole and central-cell components of the external electronic potential are "switched on" by writing

$$V_{\rm ext}^{\rm ps}(\lambda_{\rm dip},\lambda_{\rm CC}) \equiv V_{\rm ext}^{\rm ps}(0,0) + \lambda_{\rm dip}\Delta V_{\rm dip}(\mathbf{r}) + \lambda_{\rm CC}\Delta V_{\rm CC}(\mathbf{r}) \ . \tag{10}$$

When $\lambda_{\rm dip}=0=\lambda_{\rm CC}$ [Figs. 2(a) and 2(e)] a self-consistent calculation with $V_{\rm ext}({\rm Si}) \equiv V_{\rm ext}^{\rm ps}(0,0)$ as input will produce the ground-state pseudovalence charge density $\rho_{\rm Si}(\mathbf{r})$ and the screening potential $V_{\rm scr}[\rho_{\rm Si}(\mathbf{r})]$ appropriate to the lattice constant selected, while using $V_{\rm ext}^{\rm ps}(1,1)$ as input [(Figs. 2(d) and 2(h)] will produce the charge density

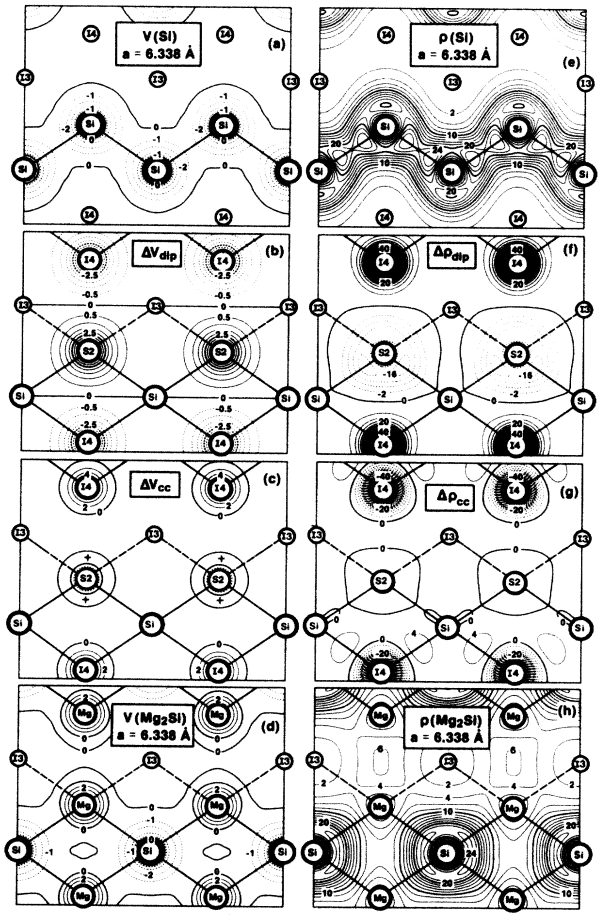

FIG. 2. Components of the external $l=0$ crystal potential (left column panels, in Ry and induced valence charge-density redistribution (right column panels, in electrons per primitive cell) for Mg_2Si in (110) plane according to decomposition of Eq. (10). All calculations are self-consistent with $K^2=32$; dashed contours indicate negative values. Straight solid lines connecting atoms indicate bonds; those connecting atoms with vacant sites are denoted as dashed straight lines. The solid rings around the atoms denote the inner core regions. See Eq. (1) for labeling of sites.

$\rho_{Mg_2Si}(\mathbf{r})$. Clearly we may now distinguish between effects due to the long-range Coulomb dipole perturbation alone and those due to central-cell effects alone: For any property of interest F (band gaps, charge densities, total energies, etc.), we may define, at fixed lattice constant, the response functions

$$\Delta F_{\rm dip}\equiv F(\lambda_{\rm dip}=1,\lambda_{CC}=0)-F(\lambda_{\rm dip}=0,\lambda_{CC}=0)\ , \tag{11a}$$

$$\Delta F_{CC}\equiv F(\lambda_{\rm dip}=1,\lambda_{CC}=1)-F(\lambda_{\rm dip}=1,\lambda_{CC}=0)\ . \tag{11b}$$

We will examine the effects of our continuous transmutation potential [Eq. (10)] on a number of quantities F [Eq. (11)] such as the band eigenvalues at high-symmetry points of the Brillouin zone common to Si, III-V's, and Mg_2Si (Sec. IV D), the ground-state valence charge density (Secs. IV B and IV C), the total energy, lattice constant, and bulk modulus (Sec. IV E).

C. Decomposition of the external crystal potential for zinc-blende compounds

Parametrizations of the sort given in Eq. (10) which retain only the valence charge differences ΔZ^v have a long and useful history in understanding the modifications in electronic structure attendant on converting, e.g., a group-IV diamond semiconductor into a "generic" III-V or II-VI one.[21–24] For this case the relevant decomposition, analogous to Eq. (10), in converting the group-IV atom at τ_l into a cation C and that at τ_2 into an anion A, is

$$V^{\rm ps}_{\rm ext}(\lambda_{\rm dip},\lambda_{CC})=V^{\rm ps}_{\rm ext}(0,0)+\lambda_{\rm dip}\Delta\tilde{V}_{\rm dip}(\mathbf{r}) +\lambda_{CC}\Delta\tilde{V}_{CC}(\mathbf{r})\ , \tag{12}$$

where

$$\Delta\tilde{V}_{\rm dip}(\mathbf{r})=\sum_{\mathbf{R}}(\Delta\tilde{Z}^{v}_{S1}/|\mathbf{r}-\mathbf{R}-\tau_1| +\Delta\tilde{Z}^{v}_{S2}/|\mathbf{r}-\mathbf{R}-\tau_2|)\ , \tag{13}$$

with $\Delta\tilde{Z}^{v}_{S1}=Z^v_C-Z^v_{\rm IV}<0$ and $\Delta\tilde{Z}^{v}_{S2}=Z^v_A-Z^v_{\rm IV}>0$, and

$$\begin{aligned}\Delta\tilde{V}_{CC}(\mathbf{r})&=\sum_{\mathbf{R}}\sum_{l}\{[v^R_{C,l}-v^R_{{\rm IV},l}](\mathbf{r}-\mathbf{R}-\tau_1) +[v^R_{A,l}-v^R_{{\rm IV},l}](\mathbf{r}-\mathbf{R}-\tau_2)\}\\ &\equiv\Delta\tilde{V}^{S1}_{CC}(\mathbf{r})+\Delta\tilde{V}^{S2}_{CC}(\mathbf{r})\ .\end{aligned} \tag{14}$$

In tetrahedral binary semiconductors $C^{\rm III}A^{\rm V}$ or $C^{\rm II}A^{\rm VI}$, a slightly different decomposition which emphasizes the loss of inversion symmetry relative to the $X^{\rm IV}X^{\rm IV}$ analog is possible. Changing the origin relative to Eq. (1) to be at the bond center $(\tau_1+\tau_2)/2$, we now have anion at

$$\mathbf{b}=(\tau_2-\tau_1)/2=a(\tfrac{1}{8},\tfrac{1}{8},\tfrac{1}{8})\ ,$$

and cation at (15)

$$-\mathbf{b}=(\tau_1-\tau_2)/2=-a(\tfrac{1}{8},\tfrac{1}{8},\tfrac{1}{8})\ .$$

In the IV-IV, III-V, II-VI, and I-VII series one can divide the compounds into "horizontal" sequences (i.e., all of whose members lie in a given row of the periodic table, e.g., GeGe-GaAs-ZnSe-CuBr) and "diagonal" (or "skew") sequences (whose members come from adjacent rows of the periodic table, e.g., GeSi-GaP-ZnS-CuCl, where the first member of the sequence is a fictitious ordered $X^{\rm IV}X'^{\rm IV}$ zinc-blende compound). We can now define the on-site difference between the repulsive core potentials $V^R_{\alpha,l}(r)$ of a cation (C) or anion (A) with respect to the $X^{\rm IV}$ atom belonging to the corresponding sequence as

$$\begin{aligned}\delta_{C,l}(r)&=v^R_{C,l}(r)-v^R_{{\rm IV},C,l}(r)\ ,\\ \delta_{A,l}(r)&=v^R_{A,l}(r)-v^R_{{\rm IV},A,l}(r)\ ,\end{aligned} \tag{16}$$

where IV, C and IV, A denote the column-IV atom in the same row of the periodic table as the cation or anion, respectively. For example, for $CA=$GaAs, $\delta_{{\rm Ga},l}(r)$ is the difference between the Ga and Ge repulsive core potentials and $\delta_{{\rm As},l}(r)$ is the difference between the As and Ge repulsive core potentials, whereas for $CA=$GaP, $\delta_{{\rm Ga},l}(r)$

is again the difference between Ga and Ge repulsive potentials, whereas $\delta_{P,l}(r)$ is the difference between the repulsive potentials of P and Si. Using these definitions we can now represent the perturbations relative to the column-IV compounds in terms of a symmetric perturbation $\Delta\tilde{V}^{\rm sym}(\mathbf{r})$ and an antisymmetric perturbation $\Delta\tilde{V}^{\rm anti}(\mathbf{r})$ as

$$V_{\rm ps}^{\rm ext}(CA)=V_{\rm ps}^{\rm ext}(X^{\rm IV}X^{\rm IV})+\lambda^{\rm sym}\Delta\tilde{V}^{\rm sym}(\mathbf{r})+\lambda^{\rm anti}\Delta\tilde{V}^{\rm anti}(\mathbf{r}) , \tag{17}$$

where

$$\Delta\tilde{V}^{\rm sym}(\mathbf{r})=\Delta\tilde{V}^{\rm sym}(-\mathbf{r}) ,$$

and

$$\Delta\tilde{V}^{\rm anti}(\mathbf{r})=-\Delta\tilde{V}^{\rm anti}(-\mathbf{r}) . \tag{18}$$

The symmetric perturbation has no contribution from the dipole term, hence

$$\Delta\tilde{V}^{\rm sym}(\mathbf{r})=\tfrac{1}{2}\sum_{\mathbf{R}}\sum_{l}\{[\delta_{C,l}(\mathbf{r}-\mathbf{R}-\mathbf{b})+\delta_{A,l}(\mathbf{r}-\mathbf{R}-\mathbf{b})]+[\delta_{C,l}(\mathbf{r}-\mathbf{R}+\mathbf{b})+\delta_{A,l}(\mathbf{r}-\mathbf{R}+\mathbf{b})]\} , \tag{19}$$

while the antisymmetric perturbation has both dipole and central-cell contributions,

$$\Delta\tilde{V}^{\rm anti}(\mathbf{r})=\Delta\tilde{V}_{\rm dip}(\mathbf{r})+\tfrac{1}{2}\sum_{\mathbf{R}}\sum_{l}\{[\delta_{C,l}(\mathbf{r}-\mathbf{R}-\mathbf{b})-\delta_{A,l}(\mathbf{r}-\mathbf{R}-\mathbf{b})]-[\delta_{C,l}(\mathbf{r}-\mathbf{R}+\mathbf{b})-\delta_{A,l}(\mathbf{r}-\mathbf{R}+\mathbf{b})]\} , \tag{20}$$

where $\Delta\tilde{V}^{\rm dip}(\mathbf{r})$ is given by Eq. (13).

A few observations follow from Eqs. (17)–(20): (i) Since $v_{\alpha,l}^{R}(r)$ varies smoothly along a row in the periodic table,[18,19] $\delta_{C,l}(r)$ and $\delta_{A,l}(r)$ have opposite signs, hence for a horizontal sequence $\Delta\tilde{V}^{\rm sym}(r)$ is expected to be small; were the variations in $v_{\alpha,l}^{R}(r)$ *linear* across a row, $\Delta\tilde{V}^{\rm sym}(r)\equiv 0$ [it was assumed to be zero for both horizontal and skew series in Refs. 21(a)–21(c)]. (ii) In a horizontal sequence,

$$\delta_{C,l}(r)-\delta_{A,l}(r)=v_{C,l}^{R}(r)-v_{A,l}^{R}(r) ,$$

hence, to the extent that the anion and cation repulsive potentials are similar, the central-cell contribution to $\Delta\tilde{V}^{\rm anti}(\mathbf{r})$ [second term in Eq. (20)] is expected to be small too [again, this was assumed zero in Refs. 21(a)–21(c)]. On the other hand, for diagonal sequences, the smooth trends for the $v_{\alpha,l}^{R}(r)$ will not in general exist, and the central-cell perturbations will not necessarily be small. We will not resort to any of these approximations in our calculations.

Items (i) and (ii) above suggest that for a horizontal sequence the dipole perturbation $\Delta\tilde{V}_{\rm dip}(\mathbf{r})$ is the dominant perturbation in Eq. (17). Although we find it unnecessary to invoke this approximation in our actual calculations, we note that it has been usefully utilized in a pioneering work by Herman[21(a)] (and later by Callaway[21(b)] and Cardona[21(c)]), who argued that (excluding special cases such as the X_1 state in diamondlike systems and the X_4 spin-orbit component) the change in a band eigenvalue of a CA compound relative to its $X^{\rm IV}X^{\rm IV}$ analog in a horizontal sequence is of second order and hence scales as $|\lambda^{\rm anti}|^2$ due to the dipole perturbation (the "λ^2 low" limit[21(a)]). For a diagonal sequence the changes were of first order in $\lambda^{\rm anti}$ [see, however, Ref. 21(c) where the Γ_{15}-Γ_{15} and L_3-L_3 gaps were somewhat artificially fitted to $(1+A\lambda^2)^{1/2}$]. Within the framework we present above, the extent to which the evolution of these gaps scales with $\lambda_{\rm dip}$ or $\lambda_{\rm dip}^2$ is a direct measure of the extent to which central-cell effects are in fact negligible (since Herman took the coupling strength $\lambda^{\rm anti}$ to be proportional to $|\Delta\tilde{Z}^{v}|^2$, which will not in general be appropriate if

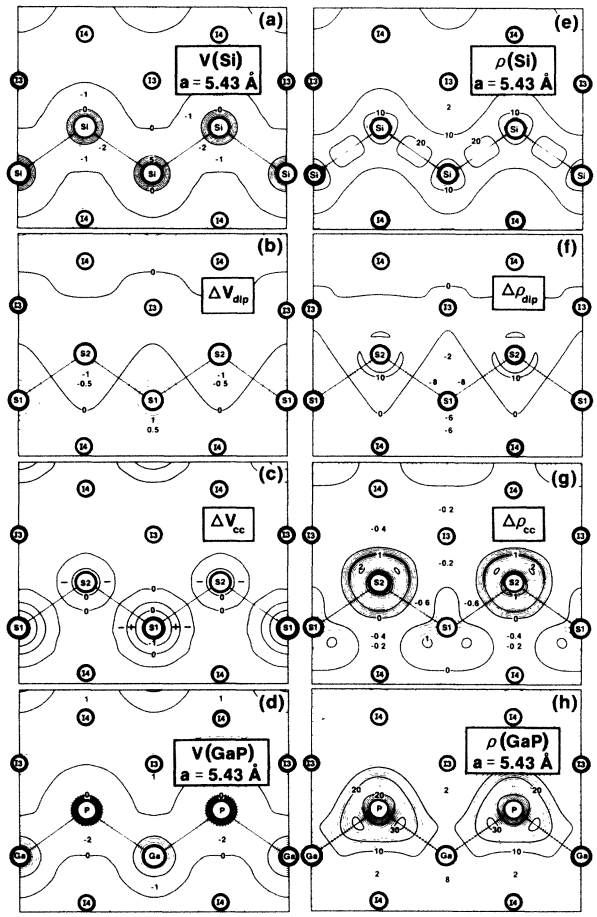

FIG. 3. Components of the $l=0$ external crystal potential (left column panels, in Ry) and the induced valence charge-density redistribution (right column panels, in electrons per primitive cell) for GaP in (110) plane according to decomposition Eq. (12). Straight lines connecting atoms indicate bonds; the solid rings around the atoms denote the inner core regions. See Eq. (1) for labeling of sites.

central-cell effects are important[25]). As another example of the utility of the generic octet semiconductor concept, we note that Phillips[22] has based his understanding of chemical trends as one proceeds away from group-IV materials on the splitting of the degeneracies of the diamond structure, i.e., the "heteropolar gaps". Furthermore, Eq. (17) has been used in the context of the empirical *local* pseudopotential method[24] to guess hitherto unknown potential form factors, e.g., the Fourier components of $\Delta\tilde{V}^{\rm sym}$ of GaAs have been approximated by those of Ge, etc. It is therefore of interest to determine how much of this splitting, for example, is *generic* to III-V compounds (i.e., a consequence of $\Delta\tilde{V}_{\rm dip}$ alone) and how much is compound *specific* (i.e., a consequence of $\Delta\tilde{V}_{\rm CC}$).

The pictorial decomposition corresponding to Eq. (12) is shown in Figs. 3(a)–3(d), calculated for CA=GaP and $a=5.431$ Å, corresponding to the experimental lattice constant of Si, close to that for GaP, $a=5.451$ Å; once again, we defer detailed description of Fig. 3 to Sec. IV. Comparison with Fig. 2, however, indicates that the situation for Mg_2Si ($\Delta Z^v_{S2}=-2$, $\Delta Z^v_{I4}=+2$) contrasts sharply with that for the more familiar case of GaP ($\Delta\tilde{Z}^v_{S1}=-1$, $\Delta\tilde{Z}^v_{S2}=+1$). In the GaP case, the dipole field $\Delta\tilde{V}_{\rm dip}(\mathbf{r})$ is *antisymmetrically* superimposed in a commensurate way on the underlying diamond lattice. This means that in generic III-V's or II-VI's the dipoles merely *redistribute* the charge associated with the IV-IV covalent bond as one switches on the dipole perturbation: No gross distortion of the ground-state charge density is necessary, precisely because no new atomic sites are being introduced in the primitive cell. However, for generic antifluorite materials the attractive dipole end resides on what was a diamond Si *interstitial* site in the absence of the dipole and the repulsive end on one of the two initial Si sites. This combination is expected to *disrupt* the Si–Si bond as the perturbation associated with $\Delta V_{\rm dip}$ is switched on, since charge is expelled from what was one end of the bond and attracted to a site where no bond existed previously; this expectation we will see borne out below.

III. COMPUTATIONAL PROCEDURE

We turn next to a description of computational details. We shall use the first-principles self-consistent pseudopotential total-energy method[26] in a plane-wave basis set used in our previous work,[3] as a natural framework for these discussions. We note, however, that effective numerical implementation of this method within a plane-wave basis relies on the use of atomic pseudopotentials whose Fourier components fall rapidly with wave vector q for large q. We have used for Mg and Si the nonlocal pseudopotential parametrizations of Bachelet, Hamann, and Schlüter.[27] Similarly, we have found it computationally convenient to "smear" the effective point charge distribution giving rise to the long-range Coulomb part of the pseudopotential decomposition Eq. (5) above; the smeared charge density

$$\rho(Z^v_\alpha,r)=Z^v_\alpha e(\beta/\pi)^{3/2}\exp(-\beta r^2) \tag{21}$$

gives rise to the smeared Coulomb (sc) pseudopotential [to be used in place of the Z^v/r term in Eq. (5)]

$$v_{\rm sc}(r)=-Z^v_\alpha\frac{e^2}{r}\,{\rm erf}(\sqrt{\beta}r) \tag{22}$$

(where erf is the error function) which has the virtues of (i) being nonsingular as $r\to 0$ and having, correspondingly, a rapid falloff for large q

$$\{=-4\pi(Z^v_\alpha e^2/q^2)\exp[-q^2/(4\beta)]\}$$

for $v_{\rm sc}(q)$, and (ii) rapidly approaching the correct $-Z^v_\alpha/r$ Coulomb behavior for large r for reasonable values of β (the choice of which will be described below). With these modifications the atomic pseudopotentials are simply decomposed, in the spirit of (5) above, as

$$w_{\alpha,l}(r)=-\frac{Z^v_\alpha}{r}{\rm erf}(\sqrt{\beta}r)+[v^R_{\alpha,l}(r)-Z^v_\alpha{\rm erfc}(\sqrt{\beta}r)]\;; \tag{23}$$

for reference later, we observe that we may write the site components of the dipole perturbation for Mg_2Si as

$$\Delta V_{\rm dip}(\mathbf{r})=\sum_{\mathbf{R}}\{(-2/|\mathbf{r}-\mathbf{R}-\tau_2|){\rm erf}(\sqrt{\beta}|\mathbf{r}-\mathbf{R}-\tau_2|)+(+2/|\mathbf{r}-\mathbf{R}-\tau_4|){\rm erf}(\sqrt{\beta}|\mathbf{r}-\mathbf{R}-\tau_4|)\}$$
$$=\Delta V^{S2}_{\rm dip}(\mathbf{r})+\Delta V^{I4}_{\rm dip}(\mathbf{r}) \tag{24}$$

and the site components of the central-cell perturbation [Eq. (9)] as

$$\Delta V^{S2}_{\rm CC}(\mathbf{r})=\sum_{\mathbf{R}}\sum_l\{[w_{{\rm Mg},l}-w_{{\rm Si},l}](\mathbf{r}-\mathbf{R}-\tau_2)-(2/|\mathbf{r}-\mathbf{R}-\tau_2|){\rm erf}(\sqrt{\beta}|\mathbf{r}-\mathbf{R}-\tau_2|)\}\;,$$
$$\Delta V^{I4}_{\rm CC}(\mathbf{r})=\sum_{\mathbf{R}}\sum_l\{w_{{\rm Mg},l}(\mathbf{r}-\mathbf{R}-\tau_4)+(2/|\mathbf{r}-\mathbf{R}-\tau_4|){\rm erf}(\sqrt{\beta}|\mathbf{r}-\mathbf{R}-\tau_4|)\}\;. \tag{25}$$

To obtain these expressions we have used the identity

$$1/r=r^{-1}[{\rm erf}(x)+{\rm erfc}(x)]$$

to express the central-cell corrections in terms of the nonsingular full l-dependent pseudopotentials for Mg and Si; the effective central-cell potentials in Eq. (25) remain of short range (for reasonable values of β) because of the cancellation of the Coulomb tails of the $w_{\alpha,l}$ with the erf terms.

The smearing parameter β has so far remained unspecified. Within the first-principles pseudopotential formalism we use one per force sacrifices a detailed knowledge of the valence electron charge density inside the core radius for a pseudized atom. It is therefore natural to

choose β so that the smeared Coulomb potential departs appreciably from $-Z_\alpha^v/r$ behavior only within such a core radius, selected to be the largest of those relevant to the atoms of interest, here Mg and Si. One might, for instance, choose β by requiring that the smeared Coulomb potential deviate from $-Z_\alpha^v/r$ by only, say, 1% at the selected core radius, obtained from a tabulation of effective orbital core radii.[28] We have used $\beta=2.44$ (a.u.)$^{-2}$, a value which closely satisfies these criteria and is identical to that used by Baur, Maschke, and Baldereschi.[23,29]

In general the kinetic energy cutoff in Ry for our plane-wave calculations is given by $E_{\rm cut}=(2\pi/a)^2K^2$, where a is the lattice constant in atomic units and K^2 is the sum of squares of integers (Miller indices) dictated by the Bravais lattice. For Si and Mg_2Si our calculations for total energy, equilibrium lattice constants, and self-consistent electronic structure were performed using kinetic energy cutoffs ($K^2=56$) corresponding to a fixed number of plane waves (459 at the Γ point of the fcc Brillouin zone, together with retention of the corresponding 3527 Fourier components of the crystal potential); this approach guarantees the absence of discontinuities in the total energy as a function of lattice constant. We have required self-consistency to better than $0.5m$ Ry; the differential convergence of the total energy across the range of lattice constants of interest (5.4 to 6.4 Å) is then better than $4m$ Ry. For these semiconductors a Brillouin zone sampling of two special **k** points[30] was used. We have used the Perdew and Zunger parametrization[31(a)] of the correlation potential due to Ceperley and Alder.[31(b)] To diagonalize the large Hamiltonian matrices resulting from the cutoffs used, we have used the residual minimization-direct inversion in the iterative subspace (RMM-DIIS) method.[32] Convergence to self-consistency of the screening potential was accelerated using the Jacobian update method.[33] In all cases we have fit our numerically determined points to the Murnaghan equation of state[34] to obtain equilibrium structural properties.

For nontrivial values of $\lambda_{\rm dip}$ and $\lambda_{\rm CC}$, the dependence of the total energy on β was such that K^2 was reduced to 32; the dependence on β for the generic III-V compound described below is considerably weaker.[35] Our expectations are that this cutoff will be adequate to describe semiquantitatively the response of the system to the perturbations above;[36] for the end-point compounds Si and Mg_2Si results are in good agreement with the more fully converged $K^2=56$ calculations;[37] equilibrium structural properties are generally less sensitive to the inclusion of high plane-wave Fourier components. On the other hand, as will be seen below, the introduction of the smeared dipole perturbation will render the system metallic; for this reason, we used a Brillouin zone sampling of 10 special **k** points[38] for values of $\lambda_{\rm dip}$ and $\lambda_{\rm CC}$ other than 1 or 0. For the end-point semiconducting compounds, once again, we find very good agreement between results for two and ten special **k**-point samplings.[39]

IV. RESULTS

A. Si and Mg_2Si

We begin our discussion by demonstrating the ability of the self-consistent local-density pseudopotential method to reproduce some of the important electronic and structural properties of the end-point materials, i.e., Si [taking $\lambda_{\rm dip}=\lambda_{\rm CC}=0$ in Eq. (10)] and Mg_2Si (taking $\lambda_{\rm dip}=\lambda_{\rm CC}=1$). In Table I we indicate the calculated and observed equilibrium lattice constants, total valence energies, and bulk moduli for Si and Mg_2Si; also shown are the results for the generic antifluorite material, discussed below. The general tendency of the local-density approximation to underestimate the equilibrium lattice constant is apparent, but agreement between experiment and theory is nonetheless reasonable. Figure 4 shows the calculated (valence) and experimental[9] (total) electronic ground-state charge densities for Mg_2Si at its experimentally observed lattice constant in the (110) plane. In particular, the "bubble" of charge density centered on the unoccupied $I3$ interstitial site [Eq. (1)] is a feature common to both figures,

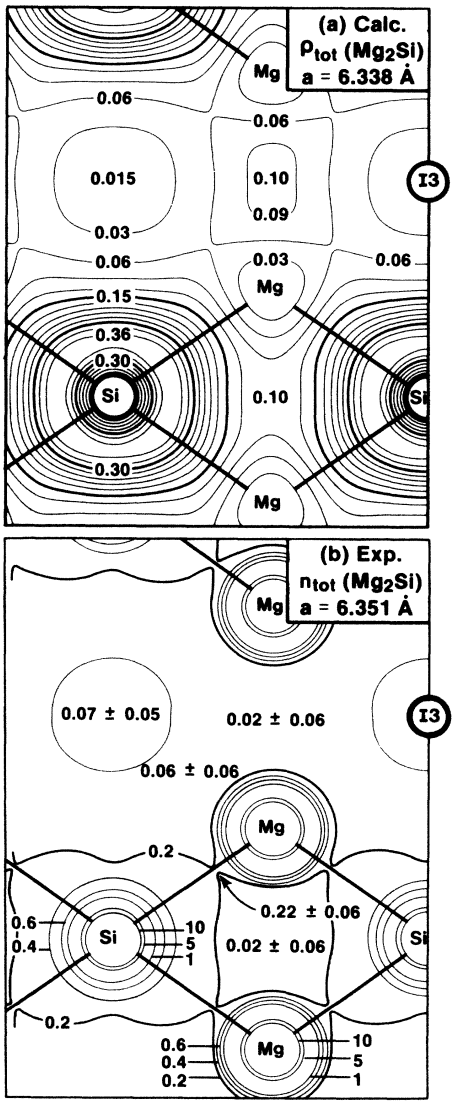

FIG. 4. Comparison of theoretically predicted valence (a) and experimentally determined (Ref. 9) total (b) charge density (in electrons per cubic Å) for Mg_2Si in (110) plane; lattice constants are 6.338 Å (a), and 6.351 Å, respectively. Straight lines connecting atoms denote bonds.

TABLE I: Calculated and observed ground-state properties of Si and Mg_2Si, and calculated results for generic antifluorite. a_{eq}, B, and E^v_{tot} denote, respectively, the equilibrium lattice constant, bulk modulus, and total valence energy. For Si and Mg_2Si a plane-wave basis set with cutoff $K^2=56$, two special **k** points, and the Ceperley-Alder (Ref. 31) exchange correlation were used. For the generic Mg_2Si (which is metallic) we use $K^2=32$ and 10 **k** points.

	Si		Mg_2Si		Generic antifluorite
Quantity	expt.	calc.	expt.	calc.	($\lambda_{dip}=1$)
a_{eq} (Å)	5.431	5.39	6.338	6.16	5.89
B (GPa)	99	114	55	68	56
E^v_{tot} (Ry/cell)		−15.869		−11.603	−12.902

and the "neck" contour half-way between the Mg and $I3$ sites is very similar in both. We find an inversion, however, of the relative charge densities on the $I3$ site and the point midway between $I3$ sites with respect to experiment. Agreement with published results of Meloni *et al.*[16(b)] is quantitative.

Table II shows the calculated band energies of Mg_2Si at high-symmetry points of the Brillouin zone; in Table III the associated transition energies (see Ref. 40 for selection rules) are compared with results of previous empirical pseudopotential calculations[14–16] and with experiment.[11–12] We calculate indirect and direct band gaps of 0.14 eV ($\Gamma_{15}\rightarrow X_{1c}$), 0.37 ($\Gamma_{15}\rightarrow X_{3c}$), and 1.90 eV ($\Gamma_{15}\rightarrow\Gamma_{1c}$), respectively, showing the well-known [e.g., Ref. 31(a)] underestimation of gaps by the local-density formalism relative to experiment (Table III).

Figure 5 depicts the calculated band structures of Si and Mg_2Si at their equilibrium zero-pressure lattice constants (5.43 and 6.34 Å, respectively), as well as for Si dilated to the lattice constant of Mg_2Si. Note the overall similarities in the band structures of Si [Fig. 5(a)] and Mg_2Si [Fig. 5(c)] at their respective equilibrium structures (except for the lifting of the double degeneracy of the Si band structure at X_1 into the $X_1+X'_4$ and X_1+X_3 states in Mg_2Si). Note further that dilation of the Si lattice constant to that of Mg_2Si results in a profoundly different band structure [Fig. 5(b)] relative to Mg_2Si [Fig. 5(c)]: The antibonding Si $3s$ band Γ'_2 which is *empty and concave upwards* in Si at equilibrium [Fig. 5(a)], becomes *occupied and concave downwards* in dilated Si [Fig. 5(b)]. This remarkable difference will be further discussed in Sec. IV D.

To understand the nature of the bonding in Mg_2Si, we show in Figs. 6 and 7 contour plots of the band-by-band charge density $|\psi_{nk}(\mathbf{r})|^2$ of some high-symmetry states. First, Fig. 6 depicts the charge densities at the two lowest valence bands at L and X, i.e., states L'_{2v}, X'_{4v}, L_{1v}, and X_{1v} [cf. Fig. 5(c)]. We note that the lowest $L_{1v}-\Gamma_{1v}-X_{1v}$ valence band is a bonding Si $3s$ band with essentially no Mg character [Figs. 6(a) and 6(b)]. This band is separated from the next $L'_{2v}-\Gamma_{15v}-X'_{4v}$ valence band by heteropolar gaps $L'_{2v}-L_{1v}$ and $X'_{4v}-X_{1v}$ at the

TABLE II. Calculated band energies of Si (both at its zero-pressure lattice constant of 5.431 Å and at the lattice constant $a=6.338$ Å of Mg_2Si) and Mg_2Si, given in eV relative to the valence band maximum. See caption to Table I for convergence parameters. Degeneracies larger than unity are shown in parentheses.

O_h^7 band label	Si $a=5.431$ Å	Si $a=6.338$ Å	Mg_2Si $a=6.338$ Å	T_d^2 band label
L'_{2v}	−9.59	−7.97	−7.67	L_{1v}
L_{1v}	−6.97	−5.52	−4.78	L'_{2v}
$L'_{3v}(2)$	−1.18	−0.81	−0.72	$L'_{3v}(2)$
L_{1c}	1.44	+0.006	1.25	L_{1c}
$L_{3c}(2)$	3.28	3.13	2.45	$L_{3c}(2)$
Γ_{1v}	−11.93	−9.38	−9.08	Γ_{1v}
$\Gamma'_{25v}(3)$	0	0	0	$\Gamma_{15v}(3)$
$\Gamma_{15c}(3)$	2.54	2.20	1.90	Γ_{1c}
Γ'_{2c}	3.23	−1.09[a]	2.41	Γ'_{25}
$X_{1v}(2)$	−7.78	−6.70	−7.12	$X_{1v'}$
			−4.43	X_{4v}
$X_{4v}(2)$	−2.82	−1.82	−1.99	$X'_{5v}(2)$
$X_{1c}(2)$	0.61	1.06	0.14	X_{1c}
			0.37	X_{3c}

[a]In valence band.

TABLE III. Comparison of calculated and observed interband transition energies in Mg_2Si, in eV.

Transition	Reflectance[a]	Electroreflectance[b]	Class	Present calculation	Au-Yang and Cohen[c]	Aymerich and Mula[d]	Lee[e]	Folland[f]
$\Gamma_{15}\rightarrow X_3$	0.6			0.37	0.53	0.49	1.3	
$\Gamma_{15}\rightarrow\Gamma_1$	2.17	2.27	M_0	1.90	2.06	1.8	2.84	2.11
$L'_3\rightarrow L_1$			M_0	1.97	2.15		3.18	2.03
$\Lambda_3\rightarrow\Lambda_1$		2.51	M_3	~2.06	2.39	2.3	3.28	
$X'_5\rightarrow X_1$	2.5		M_0	2.13	2.62		3.10	6.3
$\Delta_5\rightarrow\Delta'_2$			M_3	2.35	2.81		4.30	
$X'_5\rightarrow X_3$	2.85		M_0	2.36	2.74	2.6	3.77	1.67
$\Gamma_{15}\rightarrow\Gamma'_{25}$		3.28	M_0	2.41	2.80		3.67	
$L'_3\rightarrow L_3$			M_2	3.17	3.59	3.5	4.10	
$\Lambda_3\rightarrow\Lambda_3$			M_3	3.28	3.79		4.37	
$\Delta_5\rightarrow\Delta_1$			M_3	3.41	3.87		3.75	
$\Delta_1\rightarrow\Delta_1$			M_0	4.13	4.60			
$\Delta_1\rightarrow\Delta_1$			M_1	4.57	5.03			
$X'_4\rightarrow X_1$			M_1	4.57	5.03			

[a]Reference 12.
[b]Reference 11.
[c]Reference 15.
[d]Reference 16(a).
[e]Reference 14.
[f]Reference 13.

zone edges. The second valence band [Figs. 6(c) and 6(d)] shows the formation of weak Mg-Mg bonds, a spherical accumulation of charge in the interstitial $I3$ sites and partially-ionic (pivoting) Si-Mg bonds. The next valence band ($L'_{3v}-\Gamma_{15v}-X'_{5v}$) [Figs. 7(a), 7(b), and 7(c)] is a bonding Si $3p$ band with very little Mg $3p$ character (none for X'_{5v}); while it has the same symmetry as the analogous band in Si [Fig. 5(a)], the strong directional Si-Si bonds no longer exist in this band in Mg_2Si. The lowest $L_{1c}-\Gamma_{1c}-X_{1c}$ conduction band in Mg_2Si (Figs. 7(d), 7(e), and 7(f)] has much of its amplitude on the interstitial sites $I3$. The lowest (indirect) interband transition hence couples a Si $3p$ level [Γ_{15v} in Fig. 7(b)] with a nonbonding interstitial level [X_{1c} in Fig. 7(f)]. The second conduction band $L_{3c}-\Gamma'_{25c}-X_{3c}$ [Figs. 7(g), 7(h), and 7(i)] also shows strong bonding Mg-Mg links along the Mg chains with little charge on the interstitial $I3$ sites. The first and second conduction bands in Mg_2Si are hence complementary in terms of their amplitudes on the sites $I3$ and Mg_{I4}: The first conduction band has much of its ampli-

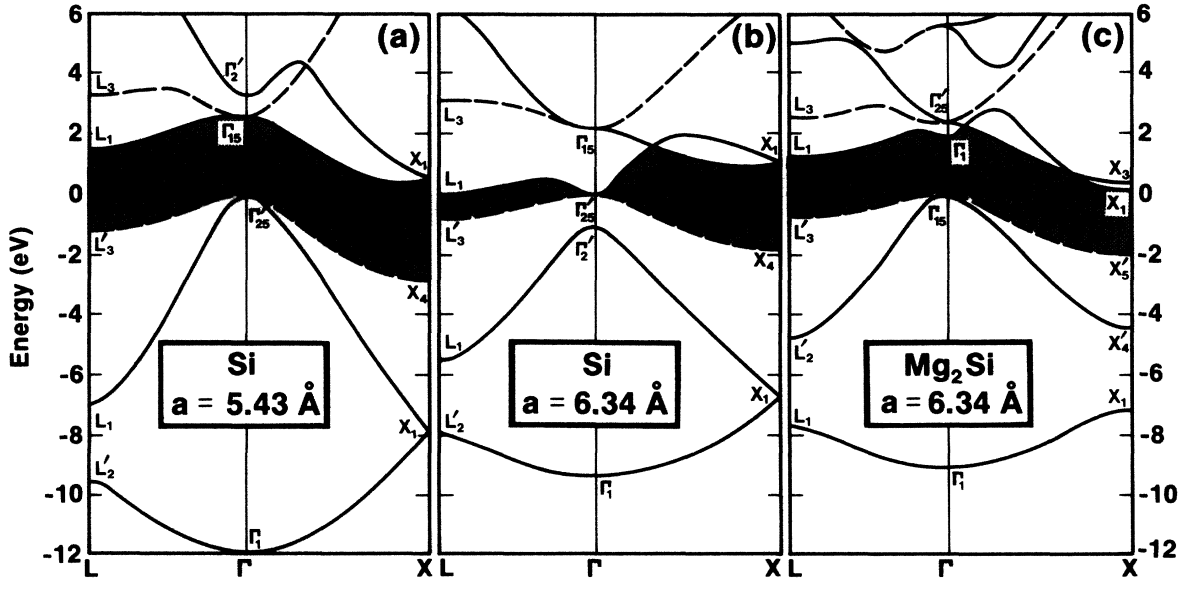

FIG. 5. Fully converged ($K^2=56$) bands of Si at $a=5.431$ Å, (a); Si at $a=6.338$ Å, (b); and Mg_2Si at $a=6.338$ Å, (c). Dashed lines indicate doubly degenerate bands. The shaded area highlights the band gap.

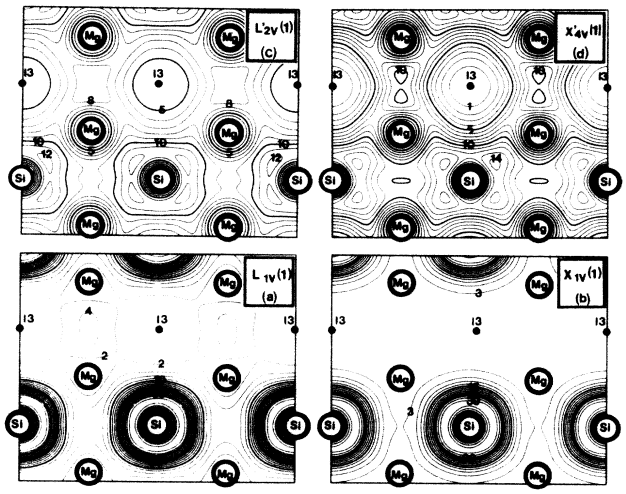

FIG. 6. Band-by-band charge-density contours (in electrons per primitive cell) for the two lowest valence bands of Mg_2Si [see Fig. 5(c)] at X and L; numbers in parentheses in state labels are band degeneracies. Solid rings indicate the inner core regions. See Eq. (1) for labeling of the sites.

tude on $I3$ but little on Mg_{I4}, whereas the second conduction band has a stronger amplitude on Mg_{I4} and little amplitude on $I3$. This feature is analogous to Si and III-V compounds.[3,4]

B. Effects on charge densities of the Si to Mg_2Si transmutation perturbation

We discuss the Si→Mg_2Si conversion via a description of its effects on the quantity central to a local-density description of the system, the ground-state electronic charge density, and of the crystal potentials which give rise to these densities. Because of the large difference in equilibrium lattice constants of these two end-point materials (Table I), we follow the evolution starting from Si dilated to the experimental lattice constant of Mg_2Si, i.e., $a=6.338$ Å. Figures 2(a), 2(b), 2(c), and 2(d) depict, respectively, the potential $V_{\rm ext}^{\rm ps}$(Si) for dilated Si, the (smeared) dipole perturbation $\Delta V_{\rm dip}$ [Eq. (8)], the central-cell perturbation $\Delta V_{\rm CC}$ [Eq. (9)], and the sum of these three contributions [Eq. (7)], i.e., the $l=0$ part of the Mg_2Si potential $V_{\rm ext}^{\rm ps}$ (Mg_2Si). The second column of Fig. 2 depicts the corresponding *response functions,* i.e., the

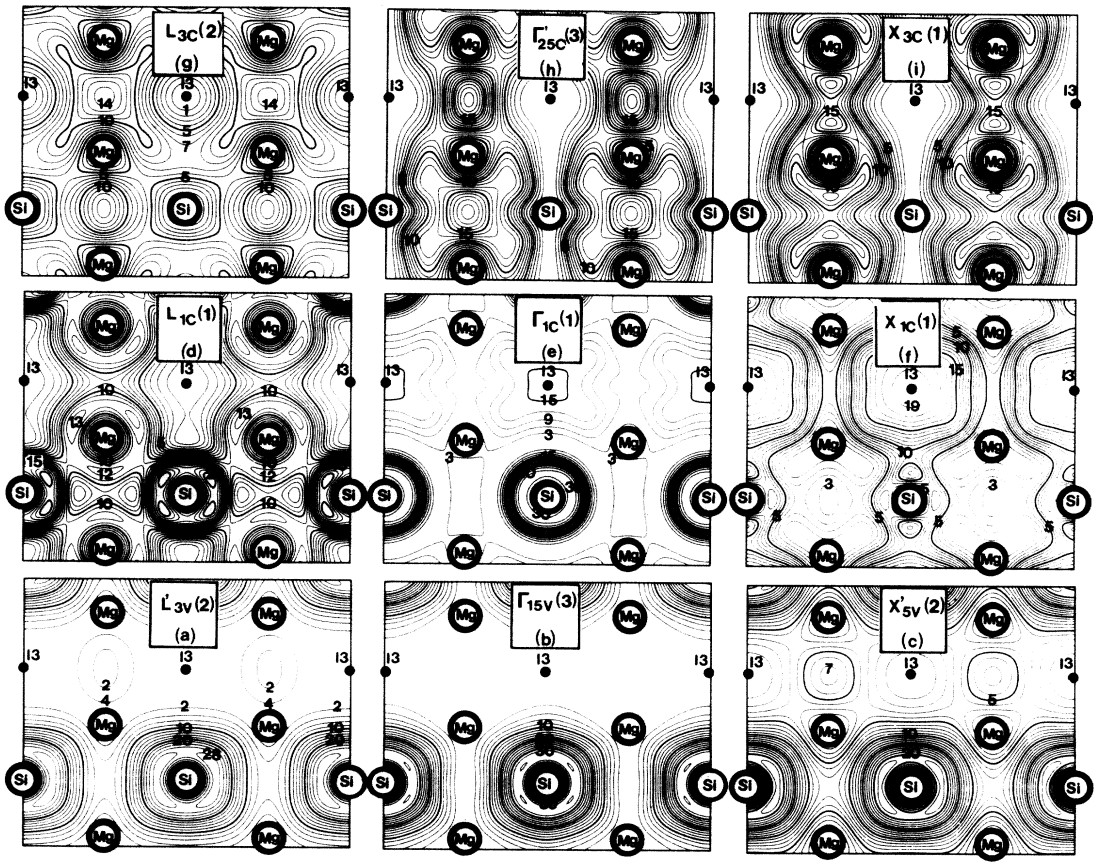

FIG. 7. Band-by-band charge-density contours for valence [(a), (b), and (c)] and conduction [(d), (e), (f), (g), (h), and (i)] bands of Mg_2Si at L, Γ, and X. See caption for Fig. 6.

self-consistently calculated charge densities, ρ(Si) [(Fig. 2(e)], the *redistribution* of valence charge induced by the dipole perturbation, i.e., $\Delta\rho_{\rm dip}$ of Eq. (11a) [Fig. 2(f)], that due to the central-cell perturbation, i.e., $\Delta\rho_{\rm CC}$ of Eq. (11b) [Fig. 2(g)], and their sum, the ground-state charge density for Mg_2Si, $\rho(Mg_2Si)$ [Fig. 2(h)]. Several remarks should be made.

(i) Figures 2(a) and 2(e) show that $\rho_{\rm Si}(\mathbf{r})$ follows the general shape of its external potential $V_{\rm ext}$(Si): There is little charge in the interstitial sites $I3$ and $I4$ and a strongly anisotropic covalent density along the chain direction. The double maxima in ρ(Si) result from the dilation of the Si-Si bond relative to its equilibrium value in Si.

(ii) Figures 2(b) and 2(f), showing the dipole perturbation and its density response, respectively, indicate the basic asymmetry of this interaction about τ_1: There is a positive potential well $\Delta V_{\rm dip}^{S2}$ at $S2$ which repels charge from it, and a symmetrically negative potential well $\Delta V_{\rm dip}^{I4}$ at $I4$ which attracts charge to it. However, since the substitutional site $S2$ in Si has more charge density than the empty interstitial site $I4$, the expulsion of charge from $S2$ far exceeds the attraction of charge to $I4$. These dipolar effects tend to powerfully disrupt the Si-Si bond (rendering the system metallic; see below) and reduce the cohesion and stiffness of the lattice, as evidenced by an increase in $a_{\rm eq}$ (by 9.3%) and a decrease in B (by -47%), discussed further in Sec. IV E.

(iii) Figures 2(c) and 2(g), showing the central-cell perturbation and its density response, respectively, indicate no symmetry or asymmetry with respect to the origin τ_1. The central-cell perturbation is of considerably shorter range than the dipolar perturbation but is complementary to it in sign: $\Delta V_{\rm CC}(\mathbf{r})$ to a large extent compensates the dipole perturbation $\Delta V_{\rm dip}(\mathbf{r})$ while preferentially depositing charge expelled from Mg_{I4} onto the Mg_{S2}-Si bond. The central-cell effect tends to further weaken the cohesion in the lattice (as evidenced by an increase in $a_{\rm eq}$ by 5%) but stiffens the bonds (B increases by 11.4%). This is further discussed in Sec. IV E.

(iv) Figures 2(d) and 2(h) show the total external potential $V_{\rm ext}(Mg_2Si)$ and its density $\rho(Mg_2Si)$. It shows that the dipole and central-cell effects nearly cancel one another around $I4$, leaving there a weak potential with little charge density: The two electrons of atomic Mg are essentially expelled from the Mg spheres leaving the system with ionic character. At the Si site, the net potential is more attractive than at the $S2$ and $I4$ Mg sites, resulting in a significant transfer of charge from Mg to Si. This disrupts the charge anisotropy around Si [evident in Fig. 2(e)]. This charge transfer from Mg results also in weak Mg-Mg metallic bonds and an increase in the effective size of the Si atoms; the covalent structure of Si [Fig. 2(e)] with substantial bond charge is replaced by an ioniclike structure in Mg_2Si [Fig. 2(h)] with little charge on the Si-Si bonds.

C. Effects on charge density of the Si to GaP transmutation perturbation

In Fig. 3 we show results analogous to those of Fig. 2 for the transmutation of Si (at its own experimental lattice constant, $a=5.431$ Å) into zinc-blende GaP (at the same lattice constant, close to its experimental value of 5.451 Å), using Eqs. (11)—(13) and numerical parameters as described for Fig. 2. A few observations follow.

(i) Figures 3(a) and 3(e) highlight the fact that the covalent bond density in Si is formed by expelling charge from both the inner core of the Si atoms [where $V_{\rm ext}$(Si) is repulsive] and the interstitial region into the bond region [where $V_{\rm ext}$(Si) is weakly attractive]. The anisotropy of $\rho_{\rm Si}(\mathbf{r})$ far exceeds that of $V_{\rm ext}^{\rm ps}$(Si): the weak nonspherical components of $V_{\rm ext}^{\rm ps}$(Si) powerfully attract charge to the bond region, away from the region where $V_{\rm ext}^{\rm ps}$(Si) is repulsive.

(ii) Figures 3(b) and 3(f) show the dipole perturbation and its density response. We note that the zero-potential contour of $\Delta\tilde{V}_{\rm dip}$ [Fig. 3(b)] is now a sawtooth curve bisecting the bonds of Si rather than the straight lines present for the antifluorite structure [Fig. 2(b)]; the opposite signs of $\Delta\tilde{V}_{\rm dip}$ on the cation and anion sides of the bond result in the simple redistribution of bonding charge mentioned above. Charge is hence transferred *symmetrically* from $S1$ to $S2$ and the zero charge contour passes through the bond center. Were $\Delta\tilde{V}_{\rm dip}(\mathbf{r})$ the only potential, the two atoms in the unit cells would have equal and opposite charge. Note also that the sites $I3$ and $I4$ are essentially unaffected by the dipole perturbation.

(iii) Figures 3(c) and 3(g) show the central-cell perturbation and its density response for GaP. While this perturbation clearly has a smaller magnitude than the dipolar perturbation, it is by no means negligible as previously[21] assumed. Since the attractiveness of $\Delta\tilde{V}_{\rm CC}^{S2}$ exceeds the repulsiveness of $\Delta\tilde{V}_{\rm CC}^{S1}$, charge is transferred from $S1$ to $S2$. In comparing the redistribution of valence charge in $Mg_2Si\leftrightarrow Si$ to that for the $GaP\leftrightarrow Si$ transmutation, we note that $\Delta\tilde{V}_{\rm CC}$ has a far smaller effect on the ground-state charge density in the latter case—the contour interval for Fig. 3(g) (the valence charge redistribution due to $\Delta\tilde{V}_{\rm CC}$) is 20 times smaller than for Fig. 2(g). It is the weakly attractive tails of $\Delta\tilde{V}_{\rm CC}$ which are responsible for the additional charge attracted near the anion and cation sites from the generic GaP bond. It is the greatly reduced impact of the central-cell effects in III-V and II-VI compounds which is responsible for the success of the approach of Herman,[21(a)] i.e., total omission of central-cell effects, discussed above.

(iv) Figures 3(d) and 3(h) depict the total external potential $V_{\rm ext}^{\rm ps}$ (GaP) and valence charge density $\rho_{\rm GaP}(\mathbf{r})$ of GaP. This shows that whereas on site $S2$ the effects of $\Delta\tilde{V}_{\rm CC}^{S2}(\mathbf{r})$ and $\Delta\tilde{V}_{\rm dip}(\mathbf{r})$ *add up* (hence, phosphorus at $S2$ absorbs much of the charge), on site $S1$ the effects of $\Delta\tilde{V}_{\rm CC}^{S1}(\mathbf{r})$ and $\Delta\tilde{V}_{\rm dip}(\mathbf{r})$ *compensate* each other.

Our results for $\Delta\rho_{\rm dip}(\mathbf{r})$ are in semiquantitative agreement with those of Baur, Maschke, and Baldereschi.[23] Our different choices of pseudopotentials (an empirical potential was chosen in Ref. 23), exchange-correlation potential, and convergence parameters are responsible for the different contour positions between our results and theirs. The present analysis is also consistent with the nature of the parametrizations of empirical pseudopotentials of Cohen and Bergstrasser[41] for the sequence Si-AlP-MgS. . . , and with the analysis of Pickenhain and Milchev[42] within the framework of linear and nonlinear

response of the interacting electron gas for Ge. This provides the *ex post facto* justification for the emphasis we have placed above on an understanding of the *bare* external crystal pseudopotential.

D. Effects on band structure of Si to Mg_2Si transmutation

We turn next to a description of the evolution of the electronic structure of Si into that of Mg_2Si according to the decomposition of Eq. (10) above. In Fig. 8 we show the associated modifications, starting from Si, dilated to the experimental lattice constant of Mg_2Si [Fig. 8(a)], as one switches on the dipole perturbation [Fig. 8(b)], resulting in the generic antifluorite silicide bands in [Fig. 8(c)] for $\lambda_{dip}=1$. Then, for $\lambda_{dip}=1$, the remaining central-cell corrections are added [Figs. 8(d) and 8(e)], resulting, for $\lambda_{CC}=1$, in the bands of Mg_2Si [Fig. 8(f)]. Analysis of the amplitudes $|\phi_{n\mathbf{k}}(\mathbf{r})|^2$ for band index n and wave vector $\mathbf{k}$ within the Brillouin zone (see below) show the band indicated as a heavy line in this figure to be the one most chemically active during the transmutation process. The dependences on the transmutation potential of band energies at high-symmetry points of the Brillouin zone are indicated in Fig. 9. Rather than to give an exhaustive description of the modifications of electronic structure according to our decomposition of the bare crystal potential [Eq. (10)], our task below will be to understand the association between the profound changes we observe for certain bands and the distributions of wave-function amplitude for these bands in the original (diamondlike Si) material.

We begin by examining the band structure for Si ex-

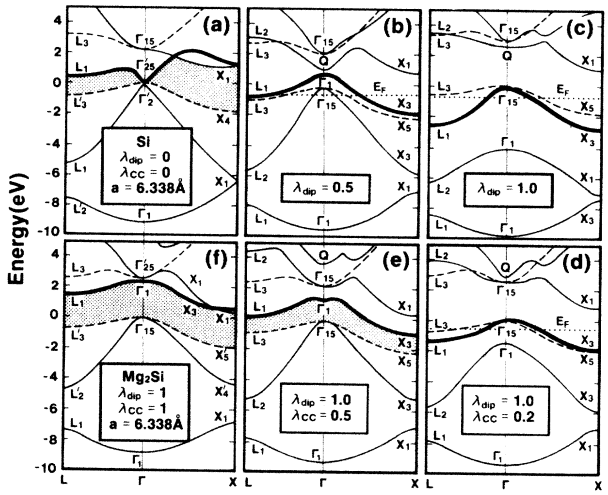

FIG. 8. Evolution of band structure of Si (dilated to experimental lattice constant of Mg_2Si into that of Mg_2Si with dipole effects (a), (b), and (c), and central-cell effects (d), (e), and (f). Dotted horizontal lines indicate Fermi energy E_F; dashed lines indicate doubly degenerate bands. Shaded areas denote the band gap between valence and conduction bands. Note the heavy solid lines which mark the most chemically active bands; Q labels a singly-degenerate state at Γ of high energy in Si and Mg_2Si.

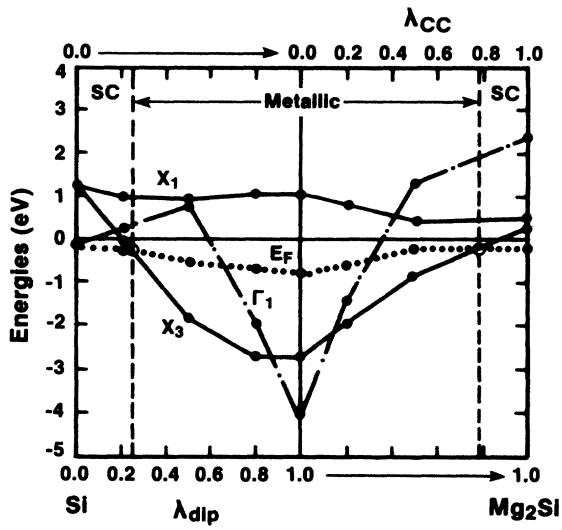

FIG. 9. Evolution with decomposition Eq. (10) of the X_1, Γ_1, and X_3 band eigenvalues. Note the ranges of metallic and semiconducting (SC) behavior. E_F denotes the Fermi energy.

panded to the experimental lattice constant of Mg_2Si [Figs. 8(a) and 5(b)]. We note that, compared with its electronic structure at its equilibrium zero-pressure lattice constant, (i) the valence bandwidth has narrowed from 11.9 to 9.4 eV, manifesting the reduced overlap of valence wave functions at the larger lattice constant; (ii) *the concave upwards conduction band with a minimum at* Γ_{2c}' *in equilibrium (undilated) Si has dropped in energy and become concave downwards near* Γ_2' *upon dilating the lattice;* moreover, it is now *occupied.* Si at $a=6.338$ Å is a zero-gap semiconductor whose bands resemble those of α-Sn (Refs. 43 and 44) and superficially those of the antifluorite compound Mg_2Pb (Ref. 45) (but without the associated spin-orbit splittings).

The inversion of the Γ_2' state deserves further comment. Inspection of the charge density for this state, shown in Fig. 10(b), shows it to be an antibonding s state, just as in equilibrium undilated Si [Fig. 10(a)]; this state is extremely sensitive to the lattice constant; we find its pressure (P) deformation potential $d\varepsilon_{n\mathbf{k}}/dP$, based on the calculations at $a=5.431$ and 6.338 Å, to be 8.8×10^{-6} eV/bar. A similar situation prevails in the alloy system $Hg_{1-x}Cd_xTe$, where the band analogous to that discussed above for Si moves down in energy into the valence band upon adding Hg to CdTe,[46] leading to a semiconductor/zero-gap semimetal transition at $x\simeq0.16$. Our work indicates that an inverted Γ_2'-like state can be a consequence merely of a large lattice constant and not necessarily a relativistic effect (absent in Si but important in HgTe). We think that the occurrence of an *occupied antibonding* state (almost a contradiction in terms) may have significant bearing on the stability of such systems. Musgrave[47] has attempted to explain the α-Sn (diamond) to β-Sn (body-centered tetragonal) structural phase transition by equating the strain energy for a specific distortion which carries one structure into the other to the energy required to promote electrons across the gap. However, no sign of the predicted mode softening has been found.[47,48]

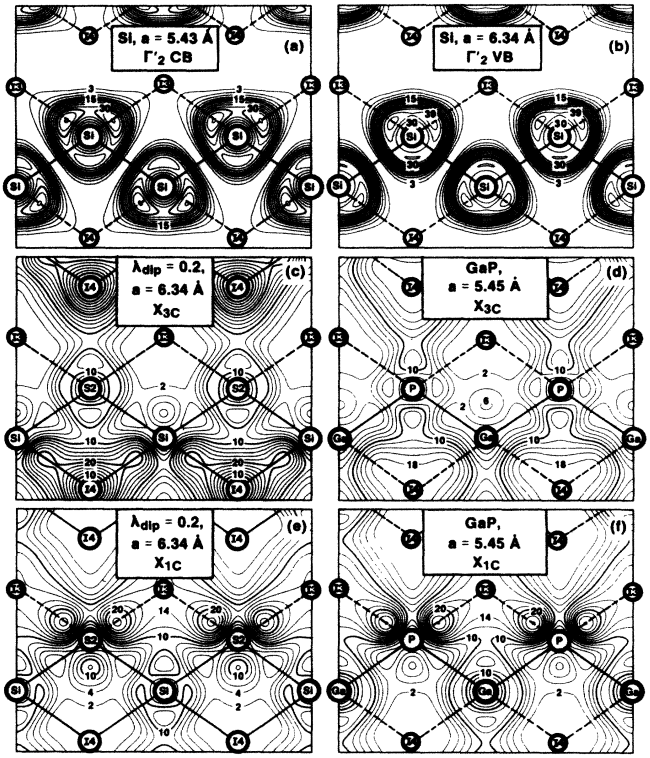

FIG. 10. Square of the wave function (in electrons per primitive cell) for Γ_2' state for Si at $a=5.431$ Å, (a) (where it is in the conduction band), and at $a=6.338$ Å, (b) (where it is in the valence band); for X_{3c} and X_{1c} states for Mg_2Si with $\lambda_{dip}=-0.2$, [(c) and (e), respectively] compared with the X_{3c} and X_{1c} states in GaP at $a=5.451$ Å [(d) and (f), respectively]. Straight lines connecting atoms denote bonds; dashed lines denote links between unoccupied (or half-occupied sites). The rings around the atoms denote the inner core regions. See Eq. (1) for the definition of the sites.

It is tempting to speculate that the predisposition of Sn (as opposed to Si and Ge) to undergo this temperature-driven transition[47,48] and the instabilities of the CdTe system upon adding Hg to it[46] are both manifestations of each system's desire to rid itself of an *occupied antibonding state.* This suggests an hitherto unrecognized simple *electronic* mechanism for the tendencies of phase changes in these systems.

Figure 9 depicts the response to the dipole plus central-cell perturbation decomposition of some selected band eigenvalues at high-symmetry points of the Brillouin zone. Turning first to the evolution of bands with the dipole perturbation, we observe that for small values of λ_{dip} ($\lesssim 0.5$) the deviations of band eigenvalues are approximately *linear.* This regime can be conceptually understood in terms of two interlinked processes: (i) the introduction of a finite value of λ_{dip} reduces the space-group symmetry from O_h^7 to T_d^2, splitting, for example, the two-fold degenerate Si X point valence and conduction bands in X_1/X_3 pairs, appropriate to the symmetry labels of the zinc-blende rather than the diamond structure; and (ii) the system then responds to the strongly attractive ΔV_{dip}^{I4} potential, first linearly, then nonlinearly, in a way dictated by the very different distributions of wave-function amplitude about the $I3$ and $I4$ tetrahedral interstitial sites, e.g., for the X_1 and X_3 zinc-blende conduction bands, described below for Figs. 10(c)—10(f).

The two-step process described above is most easily understood by reference to Fig. 10. Even for small λ_{dip} a plot of wave-function amplitude for, e.g., the second conduction band at the X point [of symmetry X_1, Fig. 10(e)] closely resembles that for the X_1 state of a genuine zinc-blende material, e.g., GaP [Fig. 10(f), with the symmetry labels dictated by a choice of origin at the Ga atom[49]], with the Si site playing the role of Ga and the Mg_{S2} site that of P. Because of the very high amplitude on the interstitial site nearest the anion in GaP [shown in Fig. 10(f)] for the X_1 state (i.e., on the attractive dipole and Mg_{I4} site for Mg_2Si), it is this state we observe to be of lower energy as the dipole strength is increased. As argued in Ref. 3, the strong selectivity between the response to perturbations centered on the interstitial site nearest the anion or on that nearest the cation for the X_1 conduction band would predict that the complementary X_3 conduction band would be only weakly perturbed by any potential centered on the Mg_{I4} site, attractive *or* repulsive: This is in accord with the weak λ_{dip} and λ_{CC} dependence of the X_3 state indicated in Fig. 9. It is in fact this high sensitivity which is responsible for the semiconductor-metal-semiconductor transitions seen in Fig. 9: The X_1 state falls through the Fermi level for $\lambda_{dip}\cong 0.25$, making the system metallic until most ($\gtrsim 75\%$) of the repulsive neon-core-like perturbation ΔV_{CC}^{I4} is present. The complete evolution of the X_3 state, starting from the X_{1c} state of dilated Si is shown in Fig. 11.

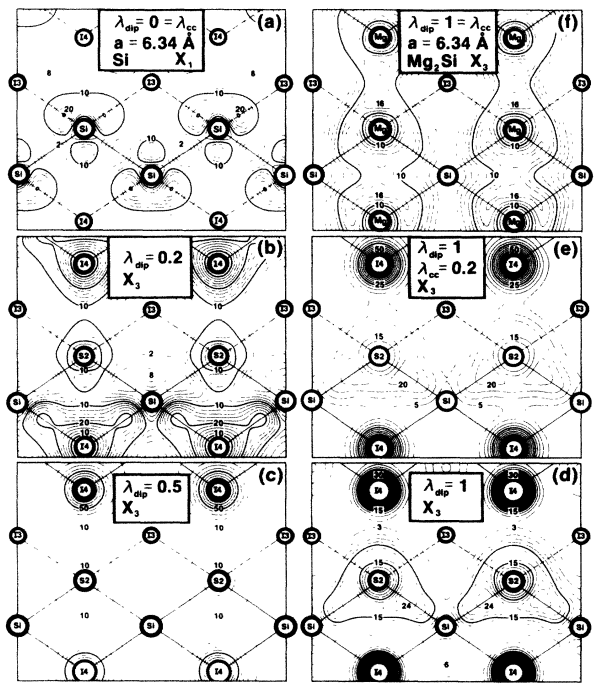

FIG. 11. Evolution of the square of the wave function for the chemically active X_3 state with λ_{dip} and λ_{CC}, Eq. (10). See caption to Fig. 10.

The nonmonotonic λ_{dip} dependence of the Γ_2'-derived state provides an interesting index to the two regimes described above: (1) linear perturbations of zinc-blende-like states derived from degeneracy-lifted Si states and (2) nonlinear effects associated with appreciable charge transfer to the Mg_{I4} site, but high amplitude (s like) around the Mg_{S2} silicon site. Thus it is sensitive to the *complementary* part of the dipole potential—the strongly repulsive Mg_{S2} end. It is for this reason that for $0 \lesssim \lambda_{dip} \lesssim 0.5$ the energy of the Γ_2'-derived state *rises* with increasing λ_{dip} (a manifestation of the "avoided crossing" principle with a higher energy band of the same symmetry). Thereafter enough charge has accumulated on the attractive Mg_{I4} site that it too begins to fall with increasing λ_{dip}, giving rise to an s-like wave function localized around the Mg_{I4} attractive dipole end until, for $\lambda_{CC} \sim 0.4$ it is expelled from the valence band. Similarly, since the Γ_2'-derived state for Mg_2Si (labeled Δ_{25}') is strongly Si s like with very low amplitude on the Mg_{S2}-Mg_{I4} sites, it is expected to fall very slowly as one subtracts the central-cell corrections, i.e., approaches the generic antifluorite case starting from the right side of Fig. 9. In fact the line segment for $\lambda_{CC}=0$, $0 \lesssim \lambda_{dip} \lesssim 0.5$ is almost parallel to that for $\lambda_{dip}=1$, $0.5 \lesssim \lambda_{CC} \lesssim 1$.

E. Equilibrium properties

1. Generic antifluorite

We next turn to a discussion of the effects of the (dipole plus central-cell) decomposition on the equilibrium lattice constant and total energy $E_{tot}(a, \lambda_{dip}, \lambda_{CC})$ of the generic antifluorite compound [Eq. (11)] corresponding to Si. In Fig. 12 we show the dependence of the total valence electron energy on lattice constant for Si, generic M_2Si and Mg_2Si. We have seen above that the dipole effects *alone* strongly disrupt the covalent bond of Si (rendering the system *metallic*, as shown in Figs. 8 and 9). Quantitatively, the effects are equally pronounced: The metallic nature of the generic antifluorite permits the lattice constant to relax by 9.3% to 5.89 Å with respect to the theoretical zero-pressure value for Si (5.39 Å in this calculation). The bulk modulus *decreases* by 47%. In going from the generic antifluorite to Mg_2Si, the lattice is dilated further (by 5%) by the insertion of what is essentially [Fig. 2(e)] a repulsive neonlike Mg core [ΔV_{CC}^{I4}, Eq. (9)], similar to the situation for He in Si or GaP.[3] The bulk modulus increases by 11.4%.

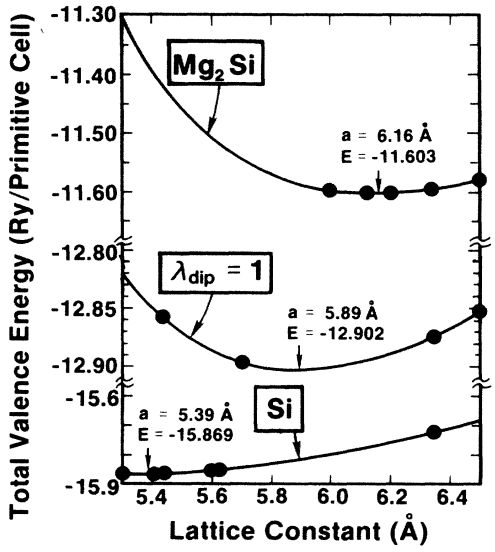

FIG. 12. Theoretical lattice constant dependence of total valence energy (in Ry) for Si ($K^2=56$), a generic antifluorite silicide (labeled $\lambda_{dip}=1$) retaining only Coulomb effects ($K^2=32$), and Mg_2Si ($K^2=56$). Note breaks in energy scales for the three curves. Vertical arrows point to the minima in the respective curves.

Using values obtained from our $K^2=32$ data, we find the smeared dipole alone (including lattice relaxation) to account for 69.5% of the change of total energy associated with the Si to Mg_2Si transmutation.

2. Generic II-VI and III-V compounds

The calculated equilibrium lattice constants of Si, generic III-V, and generic II-VI (using a fixed energy cutoff of 12 Ry, 10 special **k** points, the Hedin-Lundquist exchange correlation, and $\beta=2.44$ a.u.$^{-1}$) is 5.40, 5.44, and 5.57 Å, respectively, showing a progressive increase in lattice parameter akin to the IV-IV→III-V→II-VI sequence. The effect of the central-cell perturbation potential on the equilibrium lattice constant can be assessed by comparing the value for the generic III-V ($a_{eq}=5.44$ Å) to the values calculated[50] by the same method and input parameters for nongeneric III-V semiconductors, e.g., 5.34, 5.42, 5.57, and 5.64 Å for GaP, AlP, GaAs, and AlAs, respectively (the experimental values are 5.45, 5.45, 5.65, and 5.66 Å, respectively). This shows central-cell effects of −0.10, −0.02, 0.13, and 0.20 Å, respectively, whereas the dipole effect is 0.05 Å for the Si→generic III-V transmutation. Comparing the bulk moduli we find a general reduction in the Si (100.9 GPa)→generic III-V (93.6 GPa)→generic II-VI (62.9 GPa) series. Comparing the value of 93.6 GPa for a generic III-V to the calculated values[50] in actual III-V systems (89.7, 86.5, 72.5, and 74.5 GPa for GaP, AlP, GaAs, and AlAs, respectively), we see again a pronounced central-cell effect of softening the system. (It should be emphasized that *only* AlP is in the horizontal sequence generated by Si; agreement for, e.g., the equilibrium bond length of a generic III-V is in fact closest for AlP. GaP and AlAs are most naturally compared with a generic III-V material based on a fictitious IV-IV′ Si-Ge reference zinc-blende material, and GaAs belongs to the generic III-V in the Ge-based horizontal sequence.) We note, however, that the dipole perturbation accounts for about 70% of the change in valence total energy in going from Si to GaP. This is extremely close to the analogous value for the conversion of Si into Mg_2Si (69.5%, including lattice relaxation) despite the much larger gross redistributions of valence charge required in the latter case. A separate account of the properties of generic III-V and II-VI compounds will be published elsewhere.[25]

V. SUMMARY AND CONCLUSIONS

In this paper we have described in detail the results of the first nonempirical total-energy calculation for an antifluorite silicide. Results for the particular example chosen, Mg_2Si, are in reasonable agreement with experimental data as far as equilibrium lattice constant, zero-pressure bulk modulus, electronic structure, and ground-state valence charge density are concerned. The main thrust of our work has been to show how an interesting class of tetrahedrally coordinated antifluorite materials can be usefully regarded as members of the "filled tetrahedral structures." In order to make clear the analogies with more familiar FTS discussed in previous papers, we have used a decomposition, within a pseudopotential formalism, of the transmutation potential which transforms diamond Si into antifluorite Mg_2Si into (a) long-range Coulomb and (b) short-range (central-cell) corrections reflecting the particular characteristics of the atoms involved. Our results for this class of compounds were contrasted with those, within the same framework, for a more familiar zinc-blende semiconductor, GaP, for which the decomposition was equally satisfactory, but in which dipole effects on the ground-state valence charge density completely dominate the central-cell effects.

Our decomposition of the transmutation of Si into GaP is a natural extension of the earlier works of, e.g., Herman[21(a)] and Bauer *et al.*[23] On the other hand, arriving at Mg_2Si via dipole and central cell perturbations might appear at first glance to be rather artificial and, moreover, unconstrained since one of the original motivations for this decomposition was to understand the small X_1-X_3 conduction band splitting in Mg_2Si, implying essentially a "zero-sum" problem. However, two observations suggest that this decomposition is useful: (1) the dipole effects alone account for $\sim 70\%$ of the change of $E^{\rm tot}$ and for $\sim 65\%$ of the change in equilibrium lattice constant in going from Si to Mg_2Si, indicating that, as expected, the gross features of the bonding and charge densities are determined by the long-range, Coulomb-like tails of the transmutation potential $[V_{\rm ps}^{\rm ext}(Mg_2Si) - V_{\rm ps}^{\rm ext}(Si)]$, and (2) the changes in band eigenvalues (Fig. 9) are quite *large,* indicating that our decomposition does satisfactorily isolate large and partially compensating effects which together produce a *small* X_1-X_3 splitting but a *large* redistribution of valence charge and an associated *large* change of total valence energy.

ACKNOWLEDGMENTS

We are grateful to S. Froyen for useful discussions. This work was supported by SERI under U.S. Department of Energy Contract No. DE-AC02-83CH10093.

[1]E. Parthé, *Crystal Chemistry of Tetrahedral Structures* (Gordon and Breach, New York, 1964), Chap. 6.

[2]H. Nowotny and W. Sibert, Z. Metalkd. **33**, 391 (1941); H. Nowotny and K. Bachmayer, Monatsh. Chem. **81**, 488 (1950); **80**, 734 (1949); R. Juza, K. Langer, and K. Von Benda, Angew. Chem. Int. Ed. Engl. **7**, 360 (1968); R. Juza and F. Hund, Z. Anorg. Chem. **257**, 1 (1948).

[3]D. M. Wood, A. Zunger, and R. de Groot, Phys. Rev. B **31**, 2570 (1985).

[4]A. E. Carlsson, A. Zunger, and D. Wood, Phys. Rev. B **32**, 1386 (1985); S. H. Wei and A. Zunger, Phys. Rev. Lett. **56**, 528 (1986).

[5]F. Heusler, Verh. Dtsch. Phys. Ges. **5**, 219 (1903); J. Kübler, A. R. Williams, and C. B. Sommers, Phys. Rev. B **28**, 1745 (1983); R. A. de Groot, F. M. Mueller, P. G. van Engen, and K. H. J. Buschow, Phys. Rev. Lett. **15**, 2024 (1983).

[6]E. Zintl and G. Brauer, Z. Phys. Chem. B **20**, 245 (1933); A. Zunger, Phys. Rev. B **17**, 2582 (1978).

[7]O. Madelung, in *Landolt-Börnstein Numerical Data and Functional Relationships in Science and Technology,* New Series, Group III, edited by O. Madelung (Springer-Verlag, Berlin, 1983), Vol. 17e, pp. 163 and 432.

[8]U. Winkler, Helv. Phys. Acta **28**, 633 (1955); G. A. Stringer and R. J. Higgins, J. Appl. Phys. **41**, 489 (1970).

[9]D. Panke and E. Wölfel, Z. Kristallogr. **129**, 9 (1969).

[10]J. Tejeda and M. Cardona, Phys. Rev. B **14**, 2559 (1976).

[11]F. Vazquez, R. A. Forman, and M. Cardona, Phys. Rev. **176**, 905 (1968).

[12]W. J. Scouler, Phys. Rev. **178**, 1353 (1969).

[13]N. O. Folland, Phys. Rev. **158**, 764 (1967).

[14]P. M. Lee, Phys. Rev. **135**, A1110 (1964).

[15]M. Y. Au-Yang and M. L. Cohen, Phys. Rev. **178**, 1358 (1969).

[16](a) F. Aymerich and G. Mula, Phys. Status Solidi **42**, 697 (1970); (b) F. Meloni, E. Mooser, and A. Baldereschi, Physica (Utrecht) **117B** and **118B**, 72 (1983).

[17]P. Herzig and J. Redinger, J. Chem. Phys. **82**, 372 (1985).

[18]A. Zunger and M. L. Cohen, Phys. Rev. B **18**, 5449 (1978).

[19]A. Zunger and M. L. Cohen, Phys. Rev. B **20**, 4082 (1979).

[20]M. Jaros, *Deep Levels in Semiconductors* (Hilger, London, 1982).

[21](a) F. Herman, J. Electron. **1**, 103 (1955); (b) J. Callaway, J. Electron. **2**, 230 (1957); (c) M. Cardona and D. L. Greenaway, Phys. Rev. **131**, 98 (1963); **125**, 1291 (1961); and M. Cardona, in *Semiconductors and Semimetals,* edited by R. K. Willardson and A. C. Beer (Academic, New York, 1967), Vol. 3, p. 125.

[22]J. C. Phillips, *Bonds and Bands in Semiconductors* (Academic, New York, 1973), Chap. 2.

[23]J. Baur, K. Maschke, and A. Baldereschi, Solid State Commun. **39**, 1297 (1981); Phys. Rev. B **27**, 3720 (1983).

[24]M. L. Cohen and V. Heine, in *Solid State Physics,* edited by H. Ehrenreich, F. Seitz, and D. Turnbull (Academic, New York, 1970), Vol. 24, pp. 38.

[25]D. M. Wood and A. Zunger (unpublished).

[26]J. Ihm, A. Zunger, and M. L. Cohen, J. Phys. C **12**, 4409 (1979).

[27]G. B. Bachelet, D. R. Hamann, and M. Schlüter, Phys. Rev. B **26**, 4199 (1982).

[28]A. Zunger, Phys. Rev. B **22**, 5839 (1980).

[29]There is a complicaton associated with the choice of a finite value of β, however: we will find the total valence energy and some of the valence band positions of the generic antifluorite silicide to depend on the value of β chosen, converging [were the calculation carried to convergence with respect to the number of plane waves used in the total-energy plane-wave formalism (Ref. 26)] to the actual Coulomb potential values as $\beta \to \infty$. This dependence is weak enough, however, not to change either the qualitative or the semiquantitative conclusions we shall draw about the generic antifluorite com-

pound; it, of course, disappears for the two reference materials Si and Mg_2Si.

[30]D. J. Chadi and M. L. Cohen, Phys. Rev. B **8**, 5747 (1973).

[31](a) J. P. Perdew and A. Zunger, Phys. Rev. B **23**, 5048 (1981); (b) D. M. Ceperley and B. J. Alder, Phys. Rev. Lett. **45**, 566 (1980).

[32]D. M. Wood and A. Zunger, J. Phys. A **18**, 1343 (1985).

[33]P. Bendt and A. Zunger, Phys. Rev. B **26**, 3114 (1982).

[34]The Murnaghan equation of state is of the form $E(V) = a + bV + CV^d$; see F. D. Murnaghan, Proc. Nat. Acad. Sci. USA **30**, 244 (1944).

[35]For $\lambda_{dip}=1$ and $\lambda_{CC}=0$, with two special **k**-point sampling, $K^2=56$, and $a=6.338$ Å, the total energy decreases by ~ 0.64 Ry per primitive cell upon changing β from 2.44 to 6.0. This should be contrasted with the case of a generic III-V compound, for which (at $a=5.431$ Å, $K^2=32$, and with two special **k** points) the total energy is reduced by ~ 0.059 Ry when β changes from 2.44 to 6.0.

[36]The total energy for $\beta=2.44$ and $\lambda_{dip}=1$, $\lambda_{CC}=0$ (for two special **k** points at $a=6.338$ Å) is reduced by ~ 0.099 Ry upon increasing the cutoff K^2 from 32 to 56.

[37]For Mg_2Si the total energy (for two special **k** points) at $a=6.338$ Å is reduced by 0.049 Ry per cell in going from $K^2=32$ to $K^2=56$.

[38]The total energy, for $\lambda_{dip}=1$, $\lambda_{CC}=0$, $K^2=32$, and $\beta=2.44$, decreased by ~ 0.36 Ry upon going from two to ten special **k**-point sampling.

[39]For Mg_2Si at $a=6.338$ Å with $K^2=32$, the valence band eigenvalues at (L, Γ, X) change by ≤ 0.03 eV and E_{tot} by $\leq 10m$ Ry in changing from 2 to 10 special **k**-point sampling. For two special **k** points, over the range $a=6$ to 6.5 Å, the valence bands at (L, Γ, X) change by ≤ 0.015 eV and the total energy by $\leq 3m$ Ry in increasing K^2 from 56 to 67; the *differential* change in total energy across this range of lattice constants is $\leq 2m$ Ry due to this change of cutoff.

[40]N. O. Folland and F. Bassani, J. Phys. Chem. Solids **29**, 281 (1968).

[41]M. L. Cohen and T. K. Bergstresser, Phys. Rev. **141**, 789 (1966).

[42]R. Pickenhain and A. Milchev, Phys. Status Solidi B **77**, 571 (1976).

[43]J. R. Chelikowski and M. L. Cohen, Phys. Rev. B **14**, 556 (1978).

[44]J. Ihm and M. L. Cohen, Phys. Rev. B **23**, 1576 (1981).

[45]J. P. Van Dyke and F. Herman, Phys. Rev. B **2**, 1644 (1970).

[46]R. Dornhaus and G. Nimtz, in *Narrow Gap Semiconductors*, Vol. 98 of *Springer Tracts in Modern Physics* (Springer-Verlag, Berlin, 1983), pp. 119–300.

[47]M. J. P. Musgrave, Proc. R. Soc. Ser. A **272**, 503 (1963); Proc. Phys. Soc. London **84**, 585 (1964).

[48]D. L. Price and J. M. Rowe, Solid State Commun. **7**, 1433 (1969).

[49]T. N. Morgan, Phys. Rev. Lett. **21**, 819 (1968).

[50]S. Froyen and M. L. Cohen, Physica (Utrecht) **117&118B**, 561 (1983).

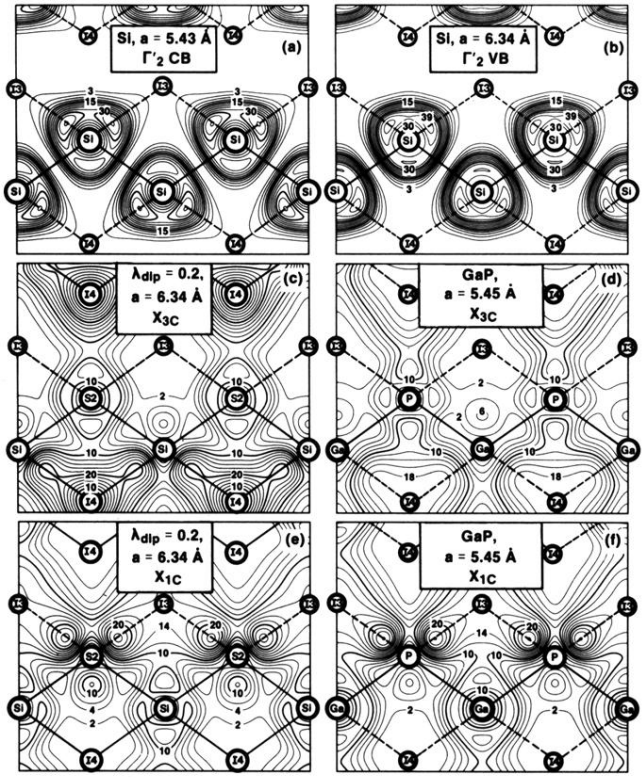

FIG. 10. Square of the wave function (in electrons per primitive cell) for Γ_2' state for Si at $a=5.431$ Å, (a) (where it is in the conduction band), and at $a=6.338$ Å, (b) (where it is in the valence band); for X_{3c} and X_{1c} states for Mg_2Si with $\lambda_{dip}=-0.2$, [(c) and (e), respectively] compared with the X_{3c} and X_{1c} states in GaP at $a=5.451$ Å [(d) and (f), respectively]. Straight lines connecting atoms denote bonds; dashed lines denote links between unoccupied (or half-occupied sites). The rings around the atoms denote the inner core regions. See Eq. (1) for the definition of the sites.

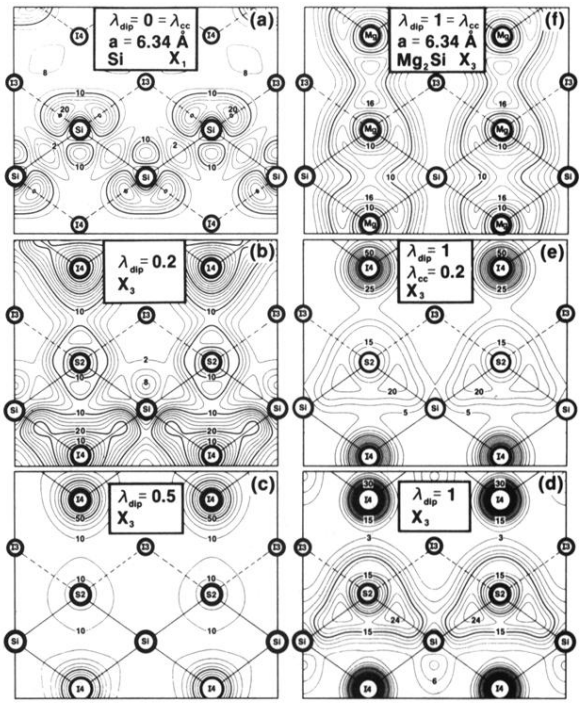

FIG. 11. Evolution of the square of the wave function for the chemically active X_3 state with λ_{dip} and λ_{CC}, Eq. (10). See caption to Fig. 10.

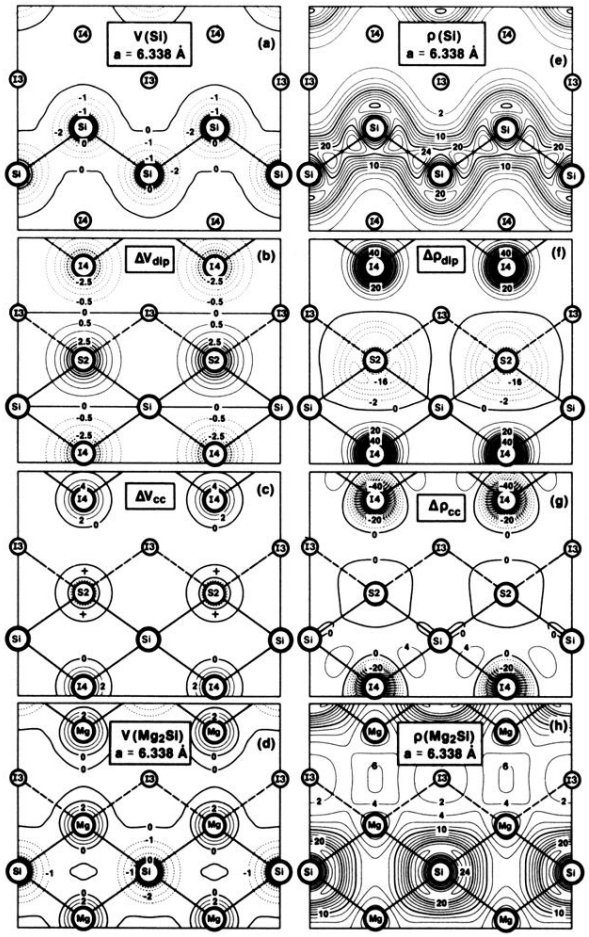

FIG. 2. Components of the external $l=0$ crystal potential (left column panels, in Ry and induced valence charge-density redistribution (right column panels, in electrons per primitive cell) for Mg_2Si in (110) plane according to decomposition of Eq. (10). All calculations are self-consistent with $K^2=32$; dashed contours indicate negative values. Straight solid lines connecting atoms indicate bonds; those connecting atoms with vacant sites are denoted as dashed straight lines. The solid rings around the atoms denote the inner core regions. See Eq. (1) for labeling of sites.

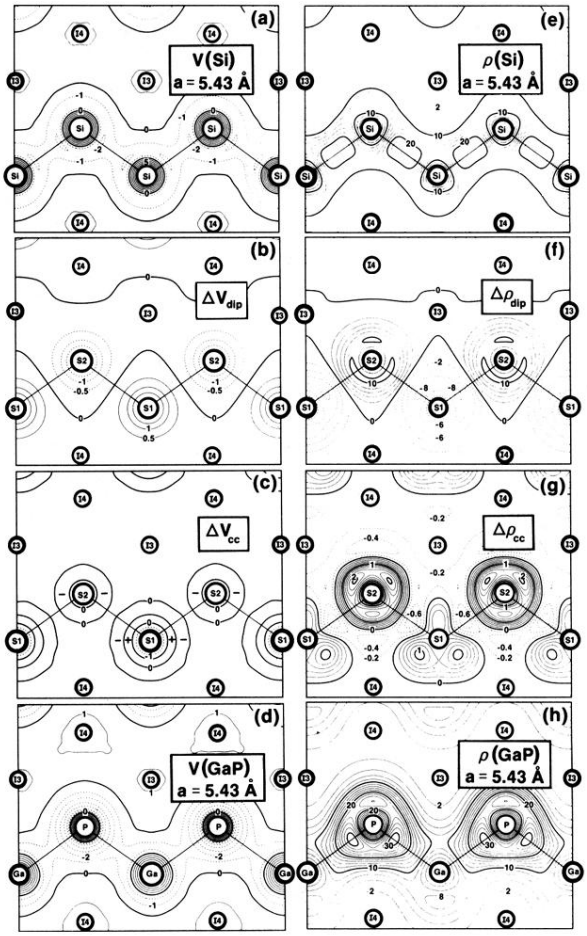

FIG. 3. Components of the $l=0$ external crystal potential (left column panels, in Ry) and the induced valence charge-density redistribution (right column panels, in electrons per primitive cell) for GaP in (110) plane according to decomposition Eq. (12). Straight lines connecting atoms indicate bonds; the solid rings around the atoms denote the inner core regions. See Eq. (1) for labeling of sites.

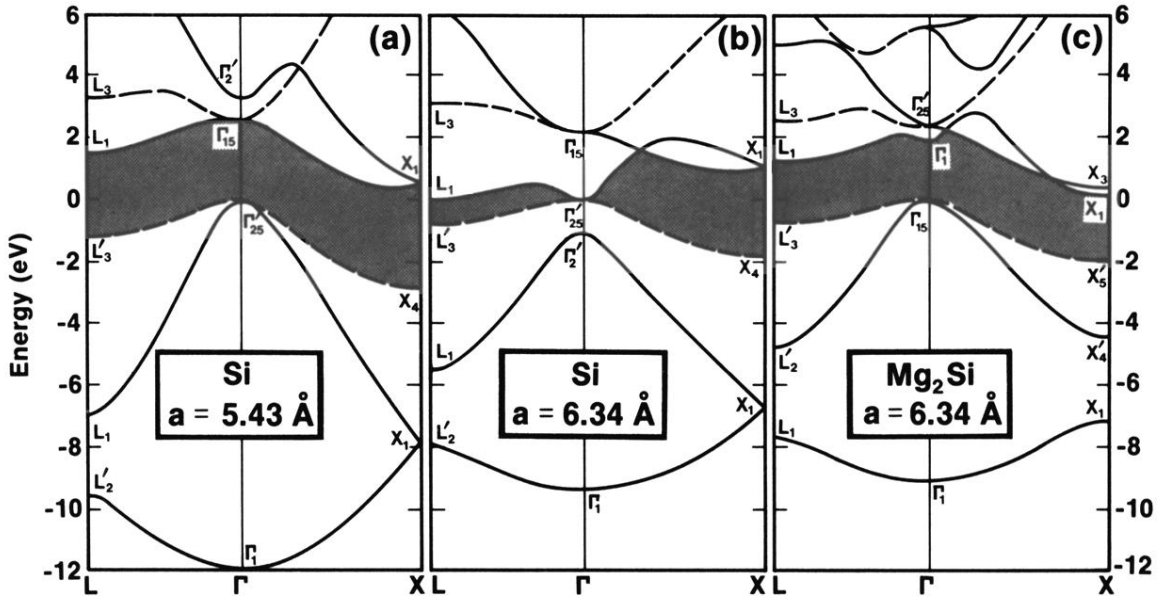

FIG. 5. Fully converged ($K^2=56$) bands of Si at $a=5.431$ Å, (a); Si at $a=6.338$ Å, (b); and Mg_2Si at $a=6.338$ Å, (c). Dashed lines indicate doubly degenerate bands. The shaded area highlights the band gap.

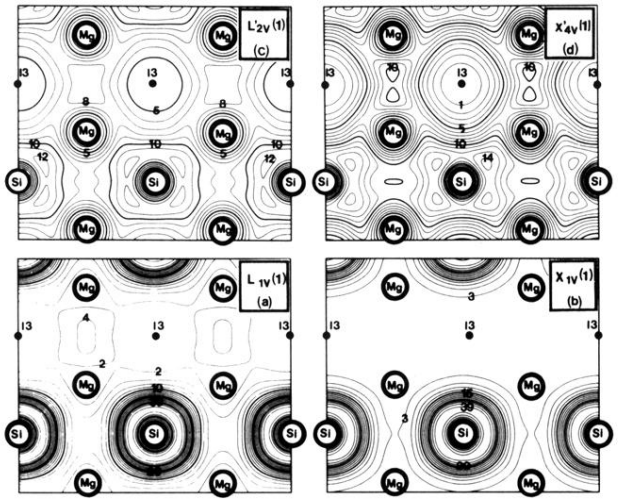

FIG. 6. Band-by-band charge-density contours (in electrons per primitive cell) for the two lowest valence bands of Mg_2Si [see Fig. 5(c)] at X and L; numbers in parentheses in state labels are band degeneracies. Solid rings indicate the inner core regions. See Eq. (1) for labeling of the sites.

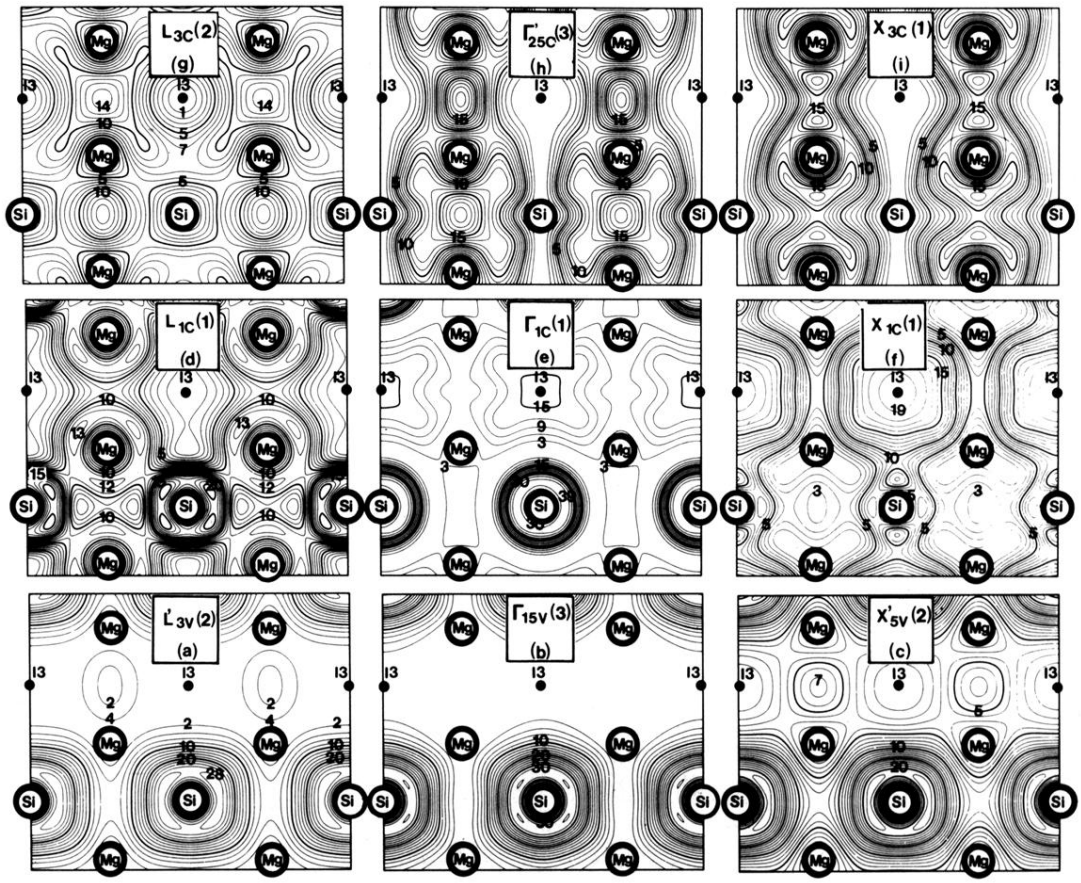

FIG. 7. Band-by-band charge-density contours for valence [(a), (b), and (c)] and conduction [(d), (e), (f), (g), (h), and (i)] bands of Mg_2Si at L, Γ, and X. See caption for Fig. 6.

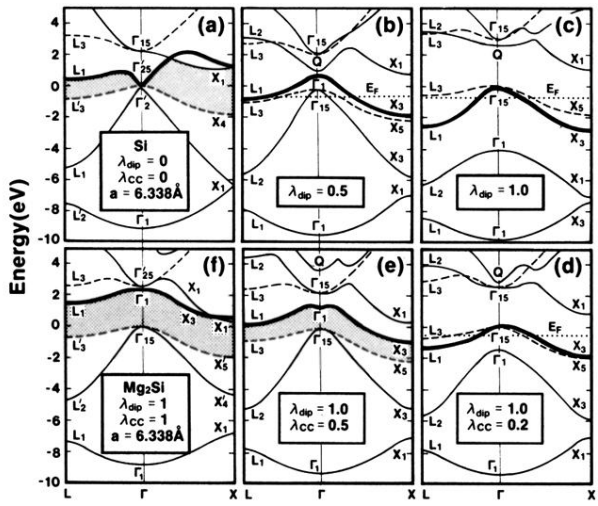

FIG. 8. Evolution of band structure of Si (dilated to experimental lattice constant of Mg_2Si into that of Mg_2Si with dipole effects (a), (b), and (c), and central-cell effects (d), (e), and (f). Dotted horizontal lines indicate Fermi energy E_F; dashed lines indicate doubly degenerate bands. Shaded areas denote the band gap between valence and conduction bands. Note the heavy solid lines which mark the most chemically active bands; Q labels a singly-degenerate state at Γ of high energy in Si and Mg_2Si.

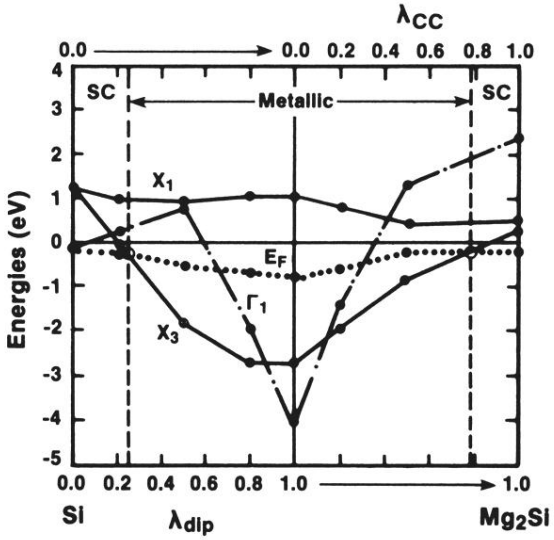

FIG. 9. Evolution with decomposition Eq. (10) of the X_1, Γ_1, and X_3 band eigenvalues. Note the ranges of metallic and semiconducting (SC) behavior. E_F denotes the Fermi energy.